Mesoporous silica adsorbents modified with amino polycarboxylate ligands – functional characteristics, health and environmental effects

Gulaim A. Seisenbaeva, Lamiaa M.A. Ali, Ani Vardanyan, Magali Gary-Bobo, Tetyana Budnyak, Vadim G. Kessler, Jean-Olivier Durand

Mesoporous silica adsorbents modified with amino polycarboxylate ligands – functional characteristics, health and environmental effects

Gulaim A. Seisenbaeva,[a]* Lamiaa M.A. Ali,[b,c,d]‡ Ani Vardanyan,[a]‡ Magali Gary-Bobo,[d] Tetyana M. Budnyak,[e,f] Vadim G. Kessler,[a] Jean-Olivier Durand [b]*

a - Department of Molecular Sciences, BioCenter, Swedish University of Agricultural Sciences, Box 7015, SE-75007, Uppsala, Sweden.
b - ICGM, Univ. Montpellier, CNRS, ENSCM, Case 1701, Place Eugène Bataillon, CEDEX 05, 34095 Montpellier (France)
c - Department of Biochemistry, Medical Research Institute, University of Alexandria, 21561 Alexandria, Egypt.
d IBMM, Univ Montpellier, CNRS, ENSCM, Montpellier. 15 Avenue Charles 9 Flahault, 34093 Montpellier Cedex 05 (France)
e - Department of Materials and Environmental Chemistry, Stockholm University, Svante Arrhenius väg 16 C, 106 91 Stockholm, Sweden
f - Chuiko Institute of Surface Chemistry of National Academy of Sciences of Ukraine, 17 General Naumov Str., 03164 Kyiv, Ukraine.

KEYWORDS: Kromasil® silica, hybrid adsorbent, REE extraction and separation, amino carboxylate ligands, health and environmental effects.

Corresponding authors:

Gulaim A. Seisenbaeva

Email: gulaim.seisenbaeva@slu.se

Postal Address: Department of Molecular Sciences, BioCenter, Swedish University of Agricultural Sciences, Almas allé 5, Box 7015, SE-75007, Uppsala, Sweden

Jean-Olivier Durand

Email: durand@univ-montp2.fr

Postal Address: Institut Charles Gerhardt de Montpellier, UMR5253, Université de Montpellier, Place EugèneBataillon, CC 1700 – Bâtiment 17, 34095 Montpellier Cedex 5, France.

ABSTRACT: A series of hybrid adsorbents were produced by surface modification with amino polycarboxylate ligands of industrially available microparticles (MP) of Kromasil® mesoporous nanostructured silica beads, bearing grafted amino propyl ligands. Produced materials, bearing covalently bonded functions as EDTA and TTHA, original Kromasil®, bearing amino propyl ligands, and bare particles, obtained by thermal treatment of Kromasil® in air, were characterized by SEM-EDS, AFM, FTIR, TGA and gas sorption techniques. Adsorption kinetics and capacity of surface-modified particles to adsorb Rare Earth Elements (REE), crucial for extraction in recycling processes, were evaluated under dynamic conditions, revealing specificity matching the ligand nature and the size of REE cations. A detailed comparison with earlier reported adsorbents for REE extraction was presented. The cytotoxicity was assessed using four different types of healthy cells, human skeletal muscles derived cells (SKMDC), fibroblast cells, macrophage cells (RAW264.7), and human umbilical vein endothelial cells (HUVECs), indicating lower toxicity of ligand-free MP than MP bearing amino poly-carboxylate functions. Internalization of the MP inside the cells and release of nitric oxide were observed. In addition, zebrafish embryos were exposed to high concentrations of MP and did not show any pronounced toxicity.

1. INTRODUCTION

Rare Earth Elements (REE) belong to the critical elements for development of modern industries. Their applications in such domains as energy production and storage, both as components in permanent magnets in wind power turbines[1] and as components in NiMH batteries[2] and as magnetic core materials for electric engines of electrically driven vehicles,[3] urges development of new sources of these elements. Both primary mining and recycling of REE require development of powerful extraction and separation techniques that need to be sustainable, not involving large amounts of hazardous reagents and solvents. As an alternative to traditionally used liquid extraction, the application of solid adsorbents has been proposed.[4] The concept of molecular recognition, earlier applied in solid adsorbents for selective removal of alkali and alkaline earth elements and exploiting crown ether ligands, has been proposed.[5] Related poly-oxygen donor ligands have been recently used on mesoporous silica matrices, showing appreciable selectivity between different members of the REE series.[6] As possible other types of ligands can be considered, for example, calixarenes. Adsorbents with calixarenes grafted on silica have been reported for removal of group I and II cation from polluted waters.[7] Free calixarenes have been used in the past as complexing ligands in solvent extraction of REE.[8] Surface-complexed REE bound to silica matric *via* calixarene functions have recently been reported as luminescent materials.[9] Other possible candidates for grafting on silica as ligands for REE extraction are poly N-donor functions discussed in a recent review.[10] These materials rely on multi-step synthesis, involving expensive ligands.

An attractive alternative in the choice of ligands for REE extraction and separation is offered by use of amino polycarboxylic acids (APCA), often referred to as complexones, which are large-scale industrial products. They have been broadly

recognized for their ability to form highly stable complexes with a broad variety of metal cations [11], and also for their active exploitation in the techniques of complexometric titration [12] and chelato-therapy [13], where ethylene diamine tetra-acetic acid (EDTA) received the main attention. In connection with the use of REE cations in magnetic resonance imaging (MRI) as contrast agents,[14] the interest has been attracted even to larger APCA ligands in REE complexes, such as diethylene triamine penta-acetic acid (DTPA) and Triethylene tetramine hexa-acetic acid (TTHA).[15-18] Later, the relatively facile grafting of these ligands on different polymers [19-21] and silica [22] colloid carriers, especially magnetic ones, made the derived hybrid materials attractive as adsorbents for advanced water purification and, more recently, for extraction and separation of REE in hydrometallurgy.[23-26] The grafting of APCA ligands occured *via* formation of an amide bond, originating from condensation of one of the carboxylic functions (Scheme 1). The capacity and selectivity of the produced hybrid adsorbent were depending on the nature of ligand. Ligands with higher number of functional groups demonstrated more pronounced capacity towards larger (lighter) REE cations.[24,27,28] Recently, the attention was attracted to produce derivatives of mesoporous silica microparticles (MP) in the view of their large surface area and large size, which permitted their use in chromatographic separation applications. Additionally, their separation became easier when magnetic components were involved.[29]

Silica has been listed as “generally recognized as safe” by the FDA.[30] For that reason, silica-based nano- or micro-particles became an attractive tool for industrial, environmental and medical applications. The toxicological behavior of nano- or micro-particles was not limited only to the chemical composition but also extended to their sizes, surface charges and shapes.[31-36] Therefore, considerable attention should be paid to studying the impact of silica-based particles on health and environment.[33-34]

In the present paper, we have further developed the surface modification approaches recently reported for industrially available mesoporous silica Kromasil® MP, carrying amino propyl functions,[29] and produced adsorbents modified with EDTA and TTHA ligands, awaiting potentially extended difference in capacity and selectivity between adsorbents bearing different ligands. The rationale of this study was based on well-demonstrated difference in capacity and selectivity of dense nanoadsorbents modified with ligands derived from EDTA, DPTA and TTHA. While they contained binding functions of the same kind, in the first hand, carboxylic groups, and tertiary amines, their mode of interaction with REE differed very significantly, because of different organization on the surface. Increase in the ligand size was observed to cause differences in the mode of surface binding for REE, resulting in pronounced selectivity towards distinct REE in the series, especially, on release.[27] In the present case, a new mode of surface ordering could be expected for mesoporous structures of Kromasil® derived materials. Morphological, structural and functional characteristics of the new materials were determined, revealing much

more complex adsorption mechanisms as compared to previously expected. Toxicological behavior of new materials was investigated on four healthy cell lines. They were selected with respect to the most probable ways of exposure and retention in the body. These particles, expected to be used in recycling of REE materials or in water purification, would potentially be able to escape into wastewaters with most probable exposure scenario being the uptake via gastrointestinal tract. The cell lines were thus represented by macrophage cells as the most common cells of the immune system, fibroblast cells as the most common cells of the connective tissue, HUVECs as model for blood vessel cells, and by skeletal muscle-derived cells to evaluate the potential retention effects.

In addition, cellular uptake and nitric oxide release were described. Moreover, *in vivo* toxicity study was conducted using zebrafish embryos as a predictive model for assessing the nano- and micro-material toxicity.[37] Obtained results were compared to those obtained using original Kromasil® and Kromasil-derived mesoporous silica deprived from organic ligands.

2. MATERIALS AND METHODS

2.1 Chemicals and agents

All chemicals used in the experiments were purchased as analytical grade reagents and used as received without further purification. All solutions were prepared in deionized water obtained from a Millipore Direct-Q3 water purification system (France). Ethylene diamine tetra-acetic acid (EDTA, anhydrous, CAS No. 60-00-4) and Triethylene tetramin hexa-acetic acid (TTHA, CAS No. 869-52-3) were purchased from Sigma Aldrich, as well as applied organic solvents, toluene and ethanol. Mesoporous Kromasil® particles (average size 10 µm, average pore size 100 Å, APTES-functionalized) were donated by AkzoNobel Special Chemicals AB, Sweden. Hydrated nitrates of REE, Lanthanum(III) nitrate hexahydrate, $La(NO_3)_3 \cdot 6H_2O$ (CAS No. 10277-43-7), Neodymium(III) nitrate hexahydrate, $Nd(NO_3)_3 \cdot 6H_2O$ (CAS No. 16454-60-7) and Dysprosium) nitrate hydrate, $Dy(NO_3)_3 \cdot xH_2O$ (CAS No. 100641-13-2) were purchased also from Sigma Aldrich. Solutions for studies of REE uptake (0.05 M) were produced by dissolving desired masses of solid nitrate salts in MilliQ water. The concentrations of REE solutions were determined by complexometric titration with EDTA using Xylenol Orange as indicator.

2.2 Functionalization

500 mg of Kromasil® (APTES-bearing) MP and 20 mL dry toluene were placed in a reaction flask and the mixture was put into an ultrasonic bath. To the produced dispersion, 100 mg of dry APCA (EDTA or TTHA) was added. The obtained solution was kept overnight under inert atmosphere at 70 °C with continuous stirring. After 24 h, the particles were separated by centrifugation (8700 rpm; 10 min), then were washed 2 times with 5 mL toluene and put into the ultrasonic bath and then

centrifuged again (8700 rpm; 10 min). Afterwards, the material was washed with 5 mL ethanol, sonicated in ultrasonic bath and was separated by centrifugation (8700 rpm; 10 min). The obtained particles were dried under nitrogen atmosphere. A portion of non-functionalized Kromasil® was heat treated at 500°C in air for 2 h to produce purely inorganic material for reference.

2.3 Uptake studies

Total uptake. 20 mg of particles were placed in a Falcon tube with 20 mL 0.010 M salt of REE and put in a shaker for 21 h. The material was then separated by centrifugation and was washed 3 times with 2.5 mL of MilliQ water. The supernatant and washing waters were united and analyzed by titration, while the particles were analyzed by Scanning Electron Microscopy / Energy Dispersive X-Ray Spectroscopy (SEM-EDS) for control estimation of adsorbed REE content.

Isotherm measurements. Stock solution of $Ln(NO_3)_3$, where Ln = La, Nd, Dy, with 0.2 M concentration was diluted for isotherm experiments. Final metal concentration was varying between 0 to 20 mM (0.5 mM, 1 mM, 5 mM, 10 mM and 20 mM). 10 mg of Kromasil-NP samples were mixed with 10 mL of metal solution in a 50 mL plastic tube and put on a shaker for 24 hours. After 24 hours the samples were centrifuged (7000 rpm) and the remaining metal concentration was determined by titration as described above. For each sample, the titrations were repeated 3 times and the average was calculated.

Kinetic experiments. 30 mg Kromasil-NP were mixed in 30 mL metal solution with initial 10 mM metal concentration. After set interval of times NPs were centrifuged (7000 rpm) for 10 min and 1 mL aliquot was separated to determine the metal concentration in the remaining solution. The sample was first diluted 10 times, and titrated afterwards.

2.4 Characterization

Particles were morphologically characterized using a SEM-EDS Hitachi TM1000-µ-DeX and Flex-SEM 1000 environmental scanning electron microscopes and a Bruker FastScan Bio atomic force microscope (AFM). Grafting of ligands was monitored with infrared spectroscopy (IR) using a Perkin-Elmer Spectrum 100 and with thermogravimetric analysis (TGA) using a Perkin-Elmer Pyris-1 instrument. Chemical composition was obtained by EDAX analysis using Hitachi Flex-SEM 1000 instrument and by elemental microanalysis performed by certified EuroFINs laboratory in Lidköping, Sweden. Specific surface areas and pore size distribution were determined from the low temperature nitrogen adsorption and desorption data. For this process, an automatic sorption analyzer ASAP 2020 (Micromeritics, USA) was used. The samples were degassed at 120 °C during 10 h before measurements. The analysis report was generated automatically using Micromeritics software (for details, please, see the Supplementary materials Tab. TS1 and text). Powder X-ray diffraction patterns of the silica nanoparticles and the Kromasil® MP were recorded

using a multifunctional Bruker D8 SMART Apex-II diffractometer operating with Mo-K_α radiation.

2.5 Cytotoxicity studies

Cell cultures. Four different healthy cell lines were used; human skeletal muscle-derived cells (SKMDCs), fibroblast cells, murine macrophage cells (RAW264.7), and human umbilical vein endothelial cells (HUVECs).

SKMDCs were maintained in F-10 nutrient medium supplemented with 25% fetal bovine serum (FBS), 1% penicillin/streptomycin (P/S), 0.1% insulin, 0.01% fibroblast growth factor (FGF), and 0.01% epidermal growth factor (EGF). Fibroblast cells were maintained in RPMI medium supplemented with 10% FBS and 1% P/S. RAW264.7 cells were maintained in Dulbecco's Modified Eagle's Medium (DMEM) supplemented with 10% FBS and 1% P/S. HUVECs were maintained in Endothelial cell Growth Medium 2 supplemented with FBS (2%), EGF (5 ng mL^{-1}), basic FGF (10 ng mL^{-1}), insulin-like growth factor (ILGF) (20 ng mL^{-1}), vascular endothelial growth factor (VEGF) (0.5 ng mL^{-1}), ascorbic acid (1 µg mL^{-1}), heparin (22.5 µg mL^{-1}), hydrocortisone (0.2 µg mL^{-1}), 1% P/S.

All cell lines were allowed to grow in humidified atmosphere at 37°C under 5% CO_2.

Cell viability assay. For cell viability experiments, cells were seeded in 96-well plate in 200 µL of their respective culture medium, 24 h after cell growth; cells were treated with different concentrations of MP and were incubated for 1, 2 and 3 days. Cells treated with the vehicle were considered as control. At the end of the incubation time, cells were incubated with 0.5 mg mL^{-1} of MTT (3-(4,5-dimethylthiazol-2-yl)-2,5-diphenyltetrazoliumbromide). Three hours after, MTT/medium solution was removed and the precipitated crystals were dissolved in ethanol/DMSO (1:1) solution with shaking for 20 min. The absorbance was measured at 540 nm. The optical density (OD) values were directly correlated with the number of living cells in well. The percentage of living cells (%) was calculated according to the following equation: OD of treated cells/ OD of control x 100

The dose-response curves were plotted as the log microparticle concentration in µg mL^{-1} versus the percentage of viable cells using Graph Pad Prism 5.0 software (San Diego, CA, USA). Data of control cells are not shown in figures as Log zero is undefined. The mean lethal concentration (LC50) was determined at 50% of cell death.

Nitric oxide (NO) measurement. RAW264.7 cells were seeded in 96-well plate in 200 µL of their respective culture medium, 24 h after cell growth; cells were treated with different concentrations of MP and were incubated for 1 day. Cells treated with the vehicle were considered as negative control. For positive control, cells were treated with 100 ng mL^{-1} of lipopolysaccharide (LPS). Nitric oxide release was measured using the Griess reagent (1% sulfanilamide, 0.1% N-[1naphthyl]-ethylenediamine

dihydrochloride, 5% phosphoric acid). After the incubation time, culture medium was collected and mixed with equal volume of Griess reagent and incubated for 15 min at room temperature in the dark. Sodium nitrite in cell culture medium was used to generate a standard curve (0 – 100 µM). Absorbance was measured at 540 nm. The concentration was calculated from the derived nitrite standard curve equation. Statistical analysis was carried out using unpaired t-test.

Cellular Uptake. Fibroblast cells were seeded in fluoroDish^{TM}, glass thickness 0.17 mm, in 1 mL of their respective culture medium. Twenty four hours after seeding, cells were treated with or without 25 µg mL^{-1} of MP and were incubated for 24 h. Cells were washed three times with their culture medium then exposed to Z-stack imaging using Zeiss LSM780 confocal fluorescence microscopy, 10x objective. Several images were taken along the Z-direction to know whether MP were present inside the cell or not. Images were treated with imageJ program.

In vivo toxicity in zebrafish embryos. Wild-type AB zebrafish strain was purchased from Zebrafish International Resource Center (ZIRC) as embryos and were raised to adulthood in circulating aquarium system inside environmentally controlled room (28 °C, 80% humidity, 14 h light/10 h dark cycle), in the lab's facilities of Molecular mechanisms in neurodegenerative dementia (MMDN), Inserm U1198, Montpellier University, Montpellier.

Fertilized embryos were collected and maintained at 28 °C. At 7 hours post fertilization (hpf), embryos were examined under the microscope, and only embryos that developed normally and reached gastrula stage were selected for the study. The 7 hpf embryos were placed in 12 well plate (20 embryos per well) and exposed to 4 mL water containing 0 or 125 or 500 mg L^{-1} of MP, concentrations were chosen according to previous toxicity studies.[38-41] The exposure to the MP was started at 7 hpf and ended at 96 hpf. The percentages of survival, mortality and hatching embryos were recorded using Loupe Olympus MVX10 stereomicroscope at 24, 48, 51, 56, 72 and 96 hpf.

Experiments with zebrafish embryos until 96 hpf are considered as *in vitro* studies according to the EU Directive 2010/63/EU on the protection of animals used for scientific purposes.[42]

3. RESULTS AND DISCUSSION

In the present study, we aimed at characterization of Kromasil based materials bearing for this system earlier not investigated functions, EDTA and TTHA, and produced their comparison with carboxylate function-free Kromasil® material.

3.1 Functional characteristics of materials

In agreement with the earlier observations on modification of Kromasil® with DTPA, the appearance of the material did not change, provided that the temperature in the course of synthesis remained low enough to avoid polymerization of the APCA

ligands (below 80°C as excessive heating results in brownish tone and strongly decreased capacity in adsorption of metal cations). The attachment of ligands occurred apparently *via* formation of an amide bond, consuming one carboxylate group per ligand moiety, as proved below by spectroscopic data (for description of underlying transformations, please, see Scheme 1). The amide bonds in grafted ligands were known to possess outstanding chemical stability. Thus for the earlier investigated DTPA-modified Kromasil the adsorption capacity was investigated in 50 consecutive cycles of uptake and release using 0.1 M nitric acid and showed a decrease of less than 1%, i.e. within the experimental margin for determination.[29] For dense particles modified with EDTA, DTPA and TTHA ligands the uptake and release by treatment with 0.1 M HNO_3 was repeated up to 5 times without any measurable loss of capacity.[27]

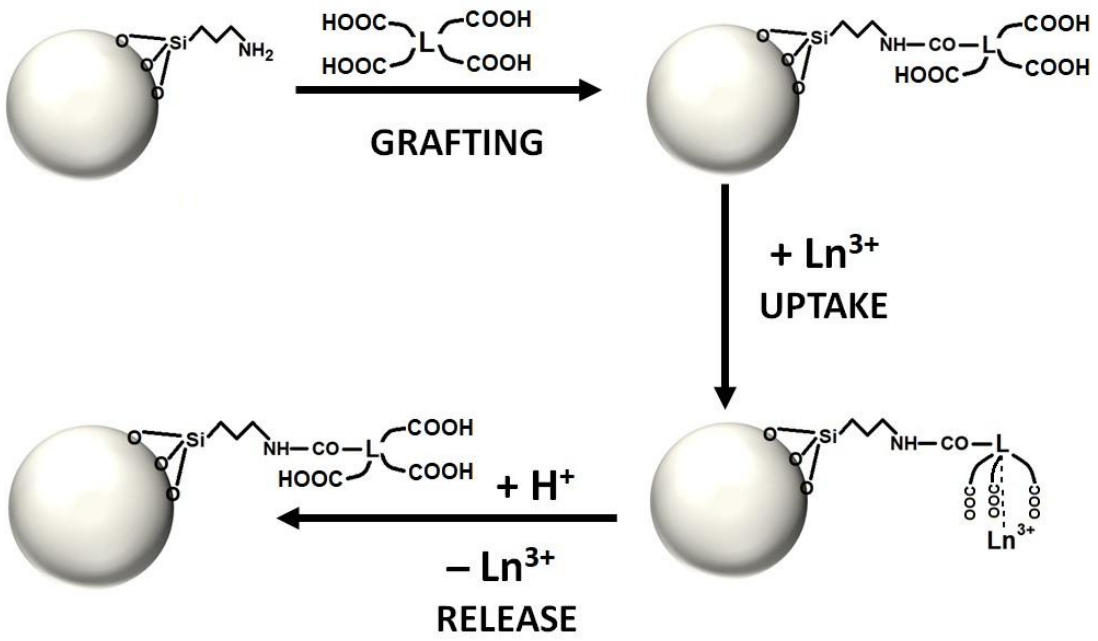

Scheme 1. Chemical transformations in surface grafting of functional ligands (L) using EDTA as example onto Kromasil particles and subsequent adsorption and desorption of REE cations.

The white powder consisted of spherical particles with the size 4 -15 µm with statistic size distribution centered at 10 µm as reported in the industrial specification, according to the SEM data (Fig. 1A-D). The microspheres were nanostructured and built up by partly coalesced small silica particles of about 20-30 nm in size according to AFM studies (Fig. 1E-H. Additionally, a full resolution AFM image is provided in Fig. FS13). The microscopic measurements were not able to distinguish the difference between ligand coverage. Grafting of ligands was easy to trace with the help of FTIR data indicating formation of amide bonds (see Scheme 1, Figs FS1-FS4). The spectrum of material annealed at 500 °C and free from organic constituents was dominated by strong bands typical for dehydrated silica, i.e. 1090 (ν_{as}(Si-O-Si)), 800 (ν(Si-O-Si)) and 460 (δ(Si-O-Si)) cm^{-1} with minor intensity bands

298 revealing presence of residual hydroxyl functions at 950 (v_{as}(Si-OH)), and δ(O-H) at
299 about 1640 cm^{-1}.

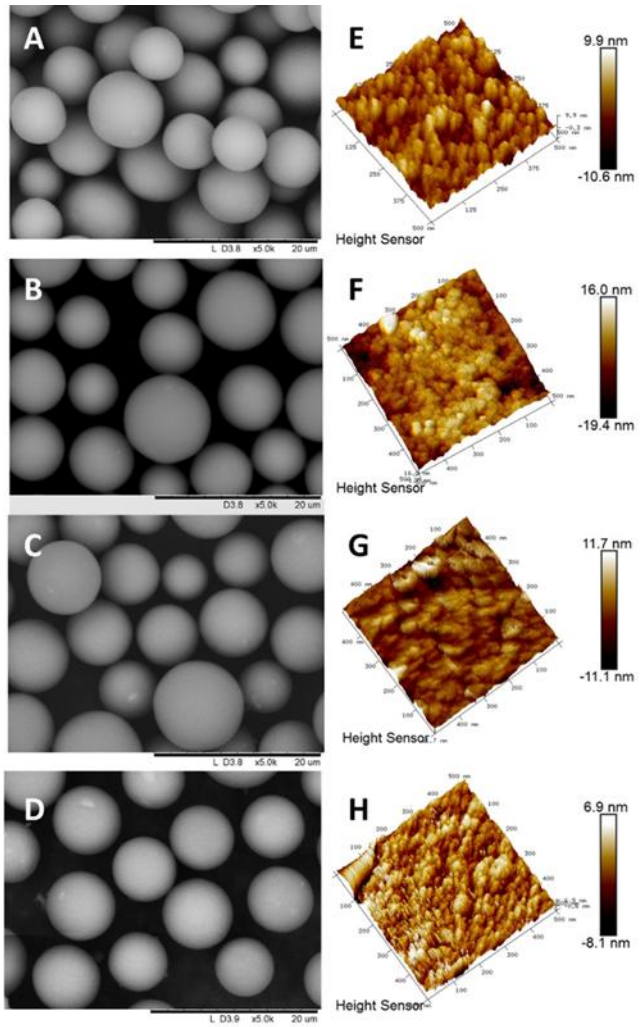

300

301 **Figure 1.** SEM and AFM images of annealed Kromasil (A, E), Kromasil® (B, F), EDTA-functionalized
302 Kromasil (C, G) and TTHA-functionalized Kromasil (D, H) respectively.

303 The spectra of initial Kromasil® and the samples modified with EDTA and TTHA
304 contained additionally protonated amine δ(N-H) at about 1470 cm^{-1} (from the
305 attached APTES function). Grafting of the amino carboxylate ligands resulted in
306 appearance of several extra bands such as, in the first hand, at 1728 cm^{-1} (ν(C=O)
307 for carboxylic acid) and about 1397 cm^{-1} (δ(O-H) of carboxylic acid). The
308 characteristic ν(C-N) band observed usually at 1250-1020 cm^{-1} was in this case
309 overlapping with intensity-saturated v_{as} (Si-O-Si) band (see Figs FS1-FS4).

310 According to TGA data (see FS5-6), the content of organic components in Kromasil®
311 was 12-14 %, where covalently bound amino propyl ligands stayed for 9-9.5 % of
312 mass loss. The EDTA-functionalized sample loses adsorbed solvents below 180 °C
313 (1.69 %) with subsequent dehydration and partial destruction, associated supposedly
314 with formation of anhydrides and amides and de-carboxylation in the temperature
315 interval 180-280°C (16.23%). Decomposition with complete destruction of ligands

occurred in the broad temperature interval 280-500 °C (12.60%) and was finally followed by burning out of the residual organic carbon at over 500 °C (3.86 %). The total weight loss of the organic ligands was 32.66%, corresponding to grafted EDTA content of 0.85 mmol/g (See Fig. FS5). For the TTHA functionalized material, the loss of solvent (14.2 %) occurred below 130 °C and was followed by first the decomposition step at around 250 °C, associated with loss of 23.1 %, then multi-step destruction with the speed maximized at around 400 °C (16.5 %), and, finally, slow burnout of residual carbon at 500-665 °C (11.4 %). This corresponded to grafted TTHA content of 2.3 mmol/g (See Fig. FS6). The ligand contents in obtained adsorbents were verified by EDAX and elemental microanalysis, basing calculations on the determined nitrogen contents as characteristic for APCA ligands (See Fig. FS7, FS8 and Tab. TS2 and TS3).

The gas sorption data revealed very distinctly the mesoporous nature of all samples, as demonstrated by characteristic type IV isotherms with hysteresis loops all featuring the H1 shape, typical of cylindrical pores formed by uniform packing of spheres featuring essentially the same size (see Fig. 2A-D).[43]

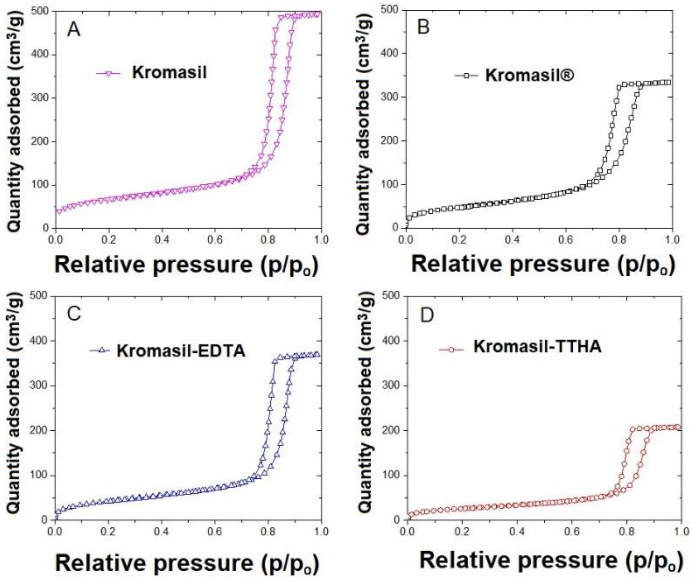

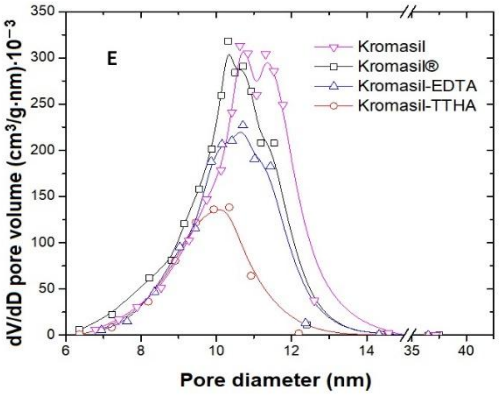

Figure 2. Nitrogen adsorption-desorption isotherms for annealed Kromasil (A), Kromasil® (B), EDTA-functionalized Kromasil (C) and TTHA-functionalized Kromasil (D), and pore size distribution for all samples (E).

This indicated that the actual shape of pores remained the same as observed by AFM and implied uniform distribution of ligands on the surface, indicating grafting in monolayer fashion. The measured active surface area was for annealed silica 243 m^2/g with pore volume 0.764 cm^3/g. The annealing lead apparently to some sintering of the constituting 20-30 nm silica blocks, possessing originally additional microporosity[29] (minor contribution with the size below cut-off limit in Fig. 2E) as for APTES-bearing Kromasil® the surface area was 188 m^2/g with somewhat smaller pore volume 0.654 cm^3/g. For the EDTA-functionalized material the surface area was about 160 m^2/g, pore volume 0.572 cm^3/g, for DTPA (this work) 177 m^2/g and 0.518 cm^3/g, and for TTHA 97 m^2/g and 0.322 cm^3/g, respectively. This corresponded well to the observed content of ligand by TGA: 0.85 mmol/g for EDTA, just below 1 mmol/g for DTPA,[29] and 2.3 mmol/g for TTHA (Textural characteristics of all materials were summarized in Supplementary Tab. TS1).

Investigation of the adsorption capacity at room temperature demonstrated that both EDTA-functionalized Kromasil and TTHA-functionalized Kromasil MP, and even Kromasil® were very efficient adsorbents. They all revealed quick kinetics of uptake with about 60% of total capacity achieved already within 1 h and maximum capacity approached in *ca.* 5 h (Fig. 3A). This was quite impressive for mesoporous materials that might otherwise require several hours (up to 72) to achieve reasonable uptake values for systems with small ordered mesopore structures.[4] Functionalized nanoparticles showed high adsorption capacity towards REE cations, with capacity related to the nature of ligand and the cation size. As it had earlier been demonstrated for monolayer complexes,[27-28] formed on the surface of dense silica particles, the ligands, possessing larger number of carboxylate groups, favored larger REE cations. This resulted in higher capacity towards lighter REE for more branched ligands.[27-28] Thus Kromasil-TTHA revealed considerably higher maximum adsorption capacity of 2.2 mmol/g towards La^{3+}-cations compared to about 1.0 mmol/g for Nd^{3+} and only 0.83 mmol/g for Dy^{3+} (Fig. 3B-D, Tab. 1). For less branched EDTA ligand the trend in adsorption capacity was reverse, i.e. 0.84 mmol/g towards La^{3+}-cations compared to about 1.2 mmol/g for Nd^{3+} and almost 1.4 mmol/g for Dy^{3+}(see Tab. 1). The uptake by unmodified Kromasil® was essentially the same and considerably lower for all three cations, in the range 0.5-0.67 mmol/g (see Fig. FS9). The maximum capacity for all three adsorbents was evaluated by complexometric titration and confirmed by EDAX mapping (see Figs. FS11, FS12). Consistent with the correlation coefficient (R^2) values, Langmuir model fitted the adsorption process better than Freundlich model. The R^2 values for Langmuir model in Nd^{3+} adsorption were 0.96 and 0.99 for Kromasil-EDTA and Kromasil-TTHA nanoparticles respectively, compared to 0.92 and 0.97 for Freundlich model (see Fig. FS 10).

Good fitting with Langmuir isotherm is generally indicative of the presence of uniform adsorption sites. In case of Kromasil-derived adsorbents in this work the adsorption capacity originated from combination of interaction with amino propyl ligands, complex formation with complexons and, possibly, even minor contribution from residual silanol functions as it had been envisaged earlier for DTPA-modified amino silica.[29,44] The capacity of non-functionalized Kromasil® in this work (0.5-0.67 mmol/g REE) was considerably higher than recently reported data for dense magnetic nanoparticles functionalized by amino propyl ligands.[45] The reason may be sought in, on one hand, smaller size of Kromasil building blocks (20-30 nm) compared to that of particles reported in ref.[45] and thus larger surface area and higher content of ligand in relation to mass of the adsorbent. On the other hand, the confinement in medium size mesopores could contribute to stability of the surface complexes. The content of amino functions on Kromasil® according to the literature[29] and the results of TGA and elemental analysis in this work was about 1.8 mmol/g. The amount of REE cations adsorbed on Kromasil® was corresponding to 1/3 of the amount of ligands, pointing at formation of $Ln(H_2NC_3H_6)_3$-type complexes with amino groups.

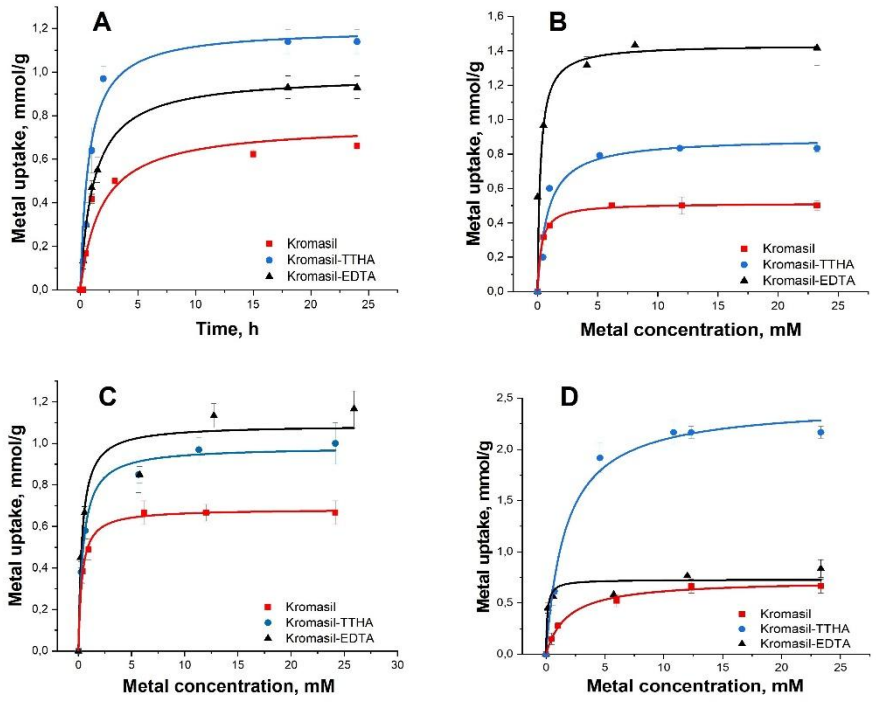

Figure 3. Kinetics of Nd^{3+}-cation adsorption on Kromasil nanoparticles modified with amino polycarboxylate ligands (A) and adsorption isotherms of Nd^{3+}(B), Dy^{3+}(C), and La^{3+}(D) cations fit by Langmuir isotherms.

This indicated that major contribution to the total adsorption capacity in modified Kromasil adsorbents was due to formation of 1:1 complexes with amino APCA-ligands. These results were also in agreement with earlier observations concerning DTPA modified Kromasil [29] and implied that complexation with these adsorbents

favored inner sphere complexation already at neutral pH, while for dense nanoparticles the major mechanism with APCA was the outer-sphere complexation associated with lower selectivity.[27] The most important novel feature was thus the observed difference in affinity, showing that EDTA and TTHA modified adsorbents possessed potentially more pronounced selectivity compared to the DTPA-modified one. The grafting of TTHA ligands, demonstrating enhanced affinity towards lighter REE, has not been reported so far to the best of our knowledge. The total capacity of the EDTA (this work) and DTPA [29] Kromasil based adsorbents lied in the range traced by Sillanpää et al. for heavy transition elements, Ni(II), Co(II) etc on APCA functionalized carbohydrate polymers.[19-21] However, in their studies they were focusing on simpler amino-modified silica gels for adsorption of REE.[46] The observed trends in selectivity and uptake were also in line with earlier results from dense surface modified silica nanoparticles,[22,26,27] but the capacity observed in the present work was considerably (50-100%) higher, especially for La^{3+} on TTHA grafted material. A remarkable feature of the adsorbents reported in the present work was also their outstanding chemical stability. In adsorption at pH 6.5 and desorption in 0.1 M HNO_3 (pH = 1) the loss of capacity was within the standard deviation of the experiments in at least 50 adsorption-desorption cycles. An important advantage of the produced materials was also their hydrophilicity, apparently facilitating diffusion of aqueous solutions and permitting their recycling at more moderate pH, compared to macroporous silica composites with crown ether or calixcrown functionalized polymers. The latter were requiring 2-5 M HNO_3 for eluating Sr(II) and La(III).[47-49] Lower concentrations of nitric acid used in renewal of the adsorbent were contributing apparently to its better stability, advantageous for potential chromatographic applications as it was traced earlier for the DTPA-functionalized Kromasil.[29]

Table 1. REE uptake by Kromasil® and EDTA and TTHA functionalized Kromasil (including Langmuir fitting parameters).

Adsorbent	Adsorption capacity, mmol/g; affinity, L/mg, R^2		
	Dy	Nd	La
Kromasil®	0.500 ± 0.05; 0.0052; 0.9993	0.667 ± 0.05; 0.0049; 0.9992	0.660 ± 0.05; 0.0022; 0.9969
Kromasil-EDTA	1.416 ± 0.15; 0.0049; 0.9996	1.166 ± 0.15; 0.0015; 0.9939	0.836 ± 0.05; 0.0021; 0.9970
Kromasil-TTHA	0.833 ± 0.05; 0.0018; 0.9970	1.041 ± 0.05; 0.0022; 0.9989	2.166 ± 0.05; 0.0013; 0.9946

For experimental details, please, see Figure FS14.

3.2 Biological experiments results

Humans are exposed to micro- and nanoparticles through different ways such as environmental contaminations, nano-remediation, spillage of nano- or micro-particles during industrial process, exposure from medical or consumer products, etc. Therefore, toxicological studies are of great importance.[35, 50] The toxicological effect related to silica exposure, especially crystalline silica (0.5 – 10 µm), on humans has

been reported.[51-52] In 1997, the IARC (International Agency for Research on Cancer) has classified crystalline silica as group 1 carcinogenic to human. Leung et al. reported the silicosis as a pathogenic consequence of inhalation of free crystalline silica in workers.[53,54] Park et al. reported that the toxicity studies of amorphous synthetic silica nano- or micro-particles were not done on large scale.[54]

Micro- and nanoparticles are internalized into the human body *via* skin contact, inhalation or ingestion, and subsequently, enter in contact with cells. Therefore, in this work it was of utmost importance to study the toxicological effect of these MP on the most representative cell populations encountered by the MP across these ways of exposure. For MP studied in this work we saw as most probable the uptake via gastro-intestinal tract and thus chose as models the macrophage cells that represented the most common cells of the immune system, fibroblast cells that represented the most common cells of the connective tissue, HUVECs that represented the blood vessel cells and skeletal muscle-derived cells. In addition, ecological risks of MP leakage into the water paths in the environment were further tested in Zebrafish embryos.

Herein, cytotoxicity in human skeletal muscle-derived cells (SKMDCs) was evaluated as a percentage of live cells, according to MTT assay, as a function of the dose and the time of treatment. Results showed the classical sigmoidal dose-response curve when plotted as a logarithmic function of MP concentration (µg mL^{-1}) versus the percentage of viable cells as shown in Fig. 4A-D. In all figures, increasing the concentration was associated with a decrease in the cell viability percentage (concentration-dependent toxicity). Also, increasing the incubation time, from 1 to 3 days, was associated with an increase in cell mortality (time-dependent toxicity).

Calculations of the LC50 values for each MP at 50% of cell death are shown in Fig. 4E. After 1 day of treatment, Kromasil grafted with EDTA and TTHA MP were more toxic, they exhibited lower LC50 values than Kromasil® and annealed Kromasil, where the LC50 values could not be detected under these conditions (>500 µg mL^{-1}). The LC50 values for all MP were decreased by days (Fig. 4E), which suggested accumulative toxic effect. In fact, after 3 days of treatment, LC50 values were 13 µg mL^{-1}, 16 µg mL^{-1}, 63 µg mL^{-1} and 71 µg mL^{-1} for Kromasil grafted with EDTA, Kromasil grafted with TTHA, Kromasil® and annealed Kromasil, respectively. All these results suggested the lower toxicity, in order, of annealed Kromasil followed by Kromasil®, Kromasil grafted with TTHA then Kromasil grafted with EDTA.

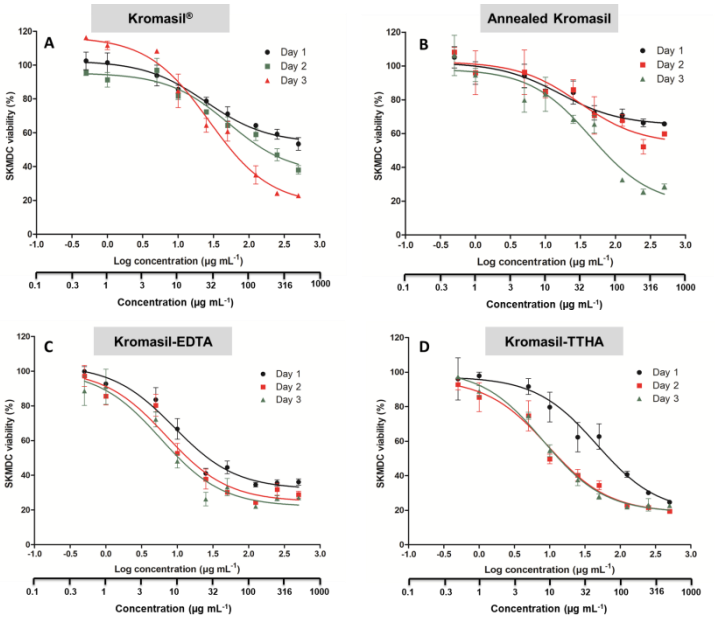

E

LC50	Kromasil®	Annealed Kromasil	Kromasil-EDTA	Kromasil-TTHA
Day 1	>500	>500	35	79
Day 2	178	500	18	18
Day 3	63	71	13	16

Figure 4. Dose-response curves representing the cell viability percentage (%) of SKMDCs treated with different concentrations of Kromasil® (A), annealed Kromasil (B), EDTA-functionalized Kromasil (C) and TTHA-functionalized Kromasil (D) for 1, 2 and 3 days. Results are presented as mean ± SEM, n=3. (E) LC50 values (as µg mL^{-1}) for all MP in SKMDCs.

Fibroblast cells were used as the most common cell type of connective tissue, the classical sigmoidal dose-response curves for all MP after 1, 2 and 3 days of treatment are shown in Fig. 5A-D, in which time- and concentration-dependent effects were observed. The LC50 values for each type of MP are shown in Fig. 5E, after 1 day of treatment, the higher LC50 value was observed for annealed Kromasil (LC50 >500 µg mL^{-1}) in compared to other MP, confirming their lower cytotoxic effect. After three days of treatment, results showed that the annealed Kromasil MP induced lower cytotoxic effect (LC50 = 141 µg mL^{-1}) than Kromasil® (LC50 = 45 µg mL^{-1}), Kromasil grafted with EDTA (LC50 = 20 µg mL^{-1}) and Kromasil grafted with TTHA MP (LC50 = 14 µg mL^{-1}).

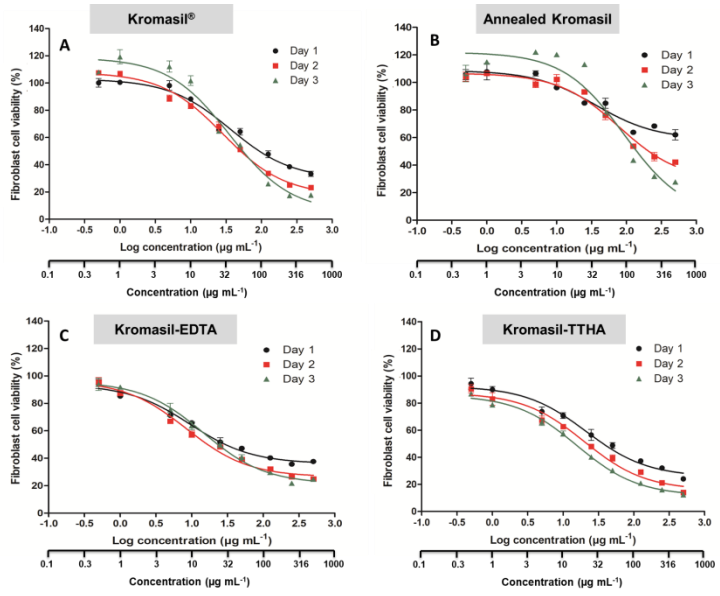

E

LC50	Kromasil®	Annealed Kromasil	Kromasil-EDTA	Kromasil-TTHA
Day 1	89	>500	32	40
Day 2	50	200	16	22
Day 3	45	141	20	14

Figure 5. Dose-response curves representing the cell viability percentage (%) of fibroblast cells treated with different concentrations of Kromasil® (A), annealed Kromasil (B), EDTA-functionalized Kromasil (C) and TTHA-functionalized Kromasil (D) for 1, 2 and 3 days. Results are presented as mean ± SEM, n=3. (E) LC50 values (as µg mL^{-1}) for all MP in fibroblast cells.

The internalization of the MP inside the cells was tested as shown in Fig. 6. Fibroblast cells were treated with a concentration lower than LC50 (25 µg mL^{-1}), results showed an obvious internalization of the MP into the cells. Internalization of MP was already observed in various studies, Serda et al. demonstrated the efficient internalization of nanoporous silicon MP (1.6 and 3.2 µm) into HUVECs with no effect on cellular integrity.[55] Also, Bimbo et al. showed the internalization of porous silicon MP (1-10 µm) in RAW264.7 macrophage cells.[56]

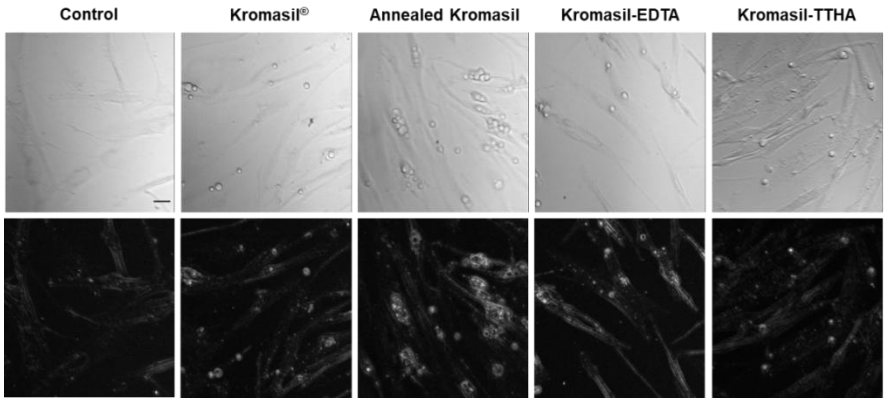

Figure 6. Z-stacking images of living fibroblasts not treated or treated with 25 µg mL^{-1} of different MP for 24 h. Scale bar 30 µm.

Macrophages are professional phagocytes with the ability to uptake any foreign particulates introduced to the body, including the exposure *via* gastro-intestinal tract. Inhaled MP caught in the nose or upper respiratory tract were demonstrated to be eliminated by macrophages or mucociliary escalator; therefore evaluation of the toxic effect of MP on macrophages was important to estimate the overall toxicity.[57] Here we studied RAW264.7 cell viability when incubated with increasing concentrations of MP during 1, 2 and 3 days (Fig. 7A-D). The LC50 values for each MP are shown in Fig. 7E. After 1 day of treatment, the LC50 values for all MP were above 250 µg mL^{-1}. These results indicated the low cytotoxic effect of all MP on macrophages in comparison with SKMDCs and fibroblast cells after 1 day of treatment. Then toxicity increased with the incubation time, and demonstrated that Kromasil® was less toxic, in order, than Kromasil grafted with EDTA, annealed Kromasil and Kromasil grafted with TTHA.

Oxidative stress is one of the mechanisms responsible for the cytotoxicity. Oxidative stress induced by nano- or MP enhances inflammation through upregulation of redox-sensitive transcription factors, including nuclear factor kappa B and activated protein 1, which induce mRNA expression of proinflammatory mediators, and finally cause inflammation.[56] Several studies showed the close relationship between reactive oxygen species production and nitric oxide (NO), a pro-inflammatory mediator that induced inflammation and a marker of oxidative stress,[58] release in RAW264.7 macrophage cells after incubation with nano- or micro-particles.[54] For this, the extracellular measurement of NO was analyzed using Griess reagent as a total nitrite concentration. Results reported in Fig. 8 showed that macrophages exhibited a significant increase in NO level when treated with Kromasil grafted with TTHA at a concentration of 125 µg mL^{-1} and above, which explained the obtained toxicity on this cell line. In case of annealed Kromasil, although it showed no induction of NO, after 1 day, an increase in the toxicity effect with time was observed, suggesting that oxidative stress was not the responsible mechanism of cell death. However, a defect in the cytoskeleton could be the cause[59] due to higher cellular uptake of these MP as observed in Figure 6.

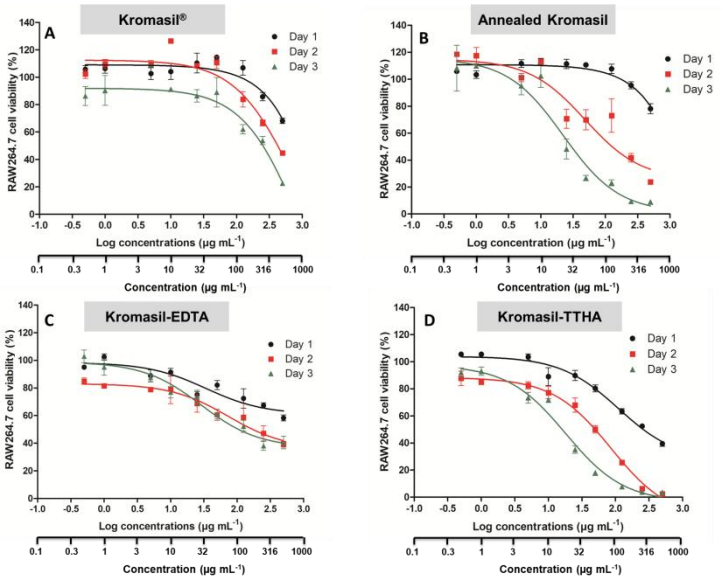

E

LC50	Kromasil®	Annealed Kromasil	Kromasil-EDTA	Kromasil-TTHA
Day 1	>500	>500	>500	282
Day 2	447	158	200	56
Day 3	251	32	126	18

Figure 7. Dose-response curves representing the cell viability percentage (%) of RAW264.7 cells treated with different concentrations of Kromasil® (A), annealed Kromasil (B), EDTA-functionalized Kromasil (C) and TTHA-functionalized Kromasil (D) for 1, 2 and 3 days. Results are presented as mean ± SEM, n=3. (E) LC50 values (as µg mL^{-1}) for all MP in RAW264.7 cells.

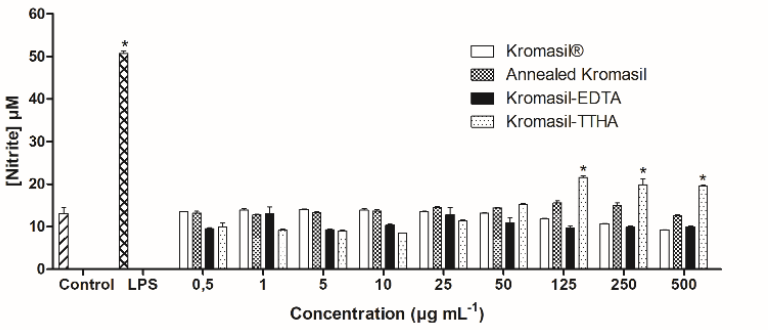

Figure 8. Extracellular measurement of nitrite concentration presents in the supernatant of RAW264.7 macrophages growth medium using Griess assay. Results are presented as mean ± SEM, n=3. Statistical analysis carried out using unpaired t-test. * Statistically significant difference from control (P<0.05).

To study the toxicological behavior of these MP on the endothelial cell function, HUVECs cell line was used, dose-response curves of HUVECs are shown in Fig. 9A-D. LC50 values were above 400 µg mL^{-1} for all MP after 1 day of treatment (Fig. 9E). The LC50 values for Kromasil® did not change by days (LC50 > 500 µg mL^{-1}) in these conditions. After 3 days of treatment, the LC50 values were 237 µg mL^{-1}, 115 µg mL^{-1} and 18 µg mL^{-1} for annealed Kromasil, Kromasil grafted with EDTA and Kromasil grafted with TTHA, respectively. These results suggested low cytotoxic

behavior of MP in HUVECs in comparison with SKMDCs, fibroblast cells and macrophages (cell-type dependent toxicity).

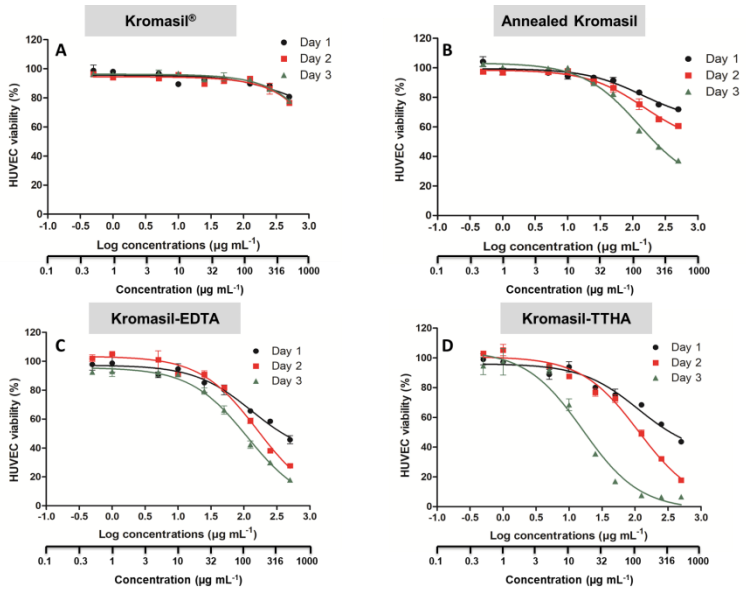

E

LC50	Kromasil®	Annealed Kromasil	Kromasil-EDTA	Kromasil-TTHA
Day 1	>500	>500	422	487
Day 2	>500	>500	178	133
Day 3	>500	237	115	18

Figure 9. Dose-response curves representing the cell viability percentage (%) of HUVECs treated with different concentrations of Kromasil® (A), annealed Kromasil (B), EDTA-functionalized Kromasil (C) and TTHA-functionalized Kromasil (D) for 1, 2 and 3 days. Results are presented as mean ± SEM, n=3. (E) LC50 values (as µg mL^{-1}) for all MP in HUVECs.

From all the above results, we could conclude that the cytotoxic behavior of the MP was concentration-, time-, cell- and ligand-dependent. An increase in toxicity was noted with the increase in microparticle concentration and time of incubation. In addition, HUVECs showed lower sensitivity toward the MP in compared to other cell lines. Finally, grafting APCA to Kromasil MP increased the cytotoxicity; it was evident that Kromasil grafted with TTHA was more toxic in all cell lines in compared to other MP, with the ability to induce inflammation in macrophages indicated by an increase in the NO level. Cytotoxicity was due to the uptake of the MP by the cells, which subsequently destabilize the cellular machinery owing to their large size.

Nano- or micro-particles will discard in the aquatic system in the form of wastewater or effluents.[60,61] Therefore, their environmental impact must be addressed. *In vivo* toxicity of MP was evaluated in zebrafish embryos. Gastrula stage embryos were exposed to water containing 0 or 125 or 500 mg L^{-1} of MP. Percentages of chorionated, dead and hatched embryos were calculated at different time points (24, 48, 51, 56, 72 and 96 hpf). Results showed that Kromasil®, annealed Kromasil and Kromasil grafted with EDTA had no toxic effect on embryos after 96 hpf of exposure

to 125 and 500 mg L^{-1} of MP, with no changes in motility, morphology and hatching rate in compared to control (Fig. 10).

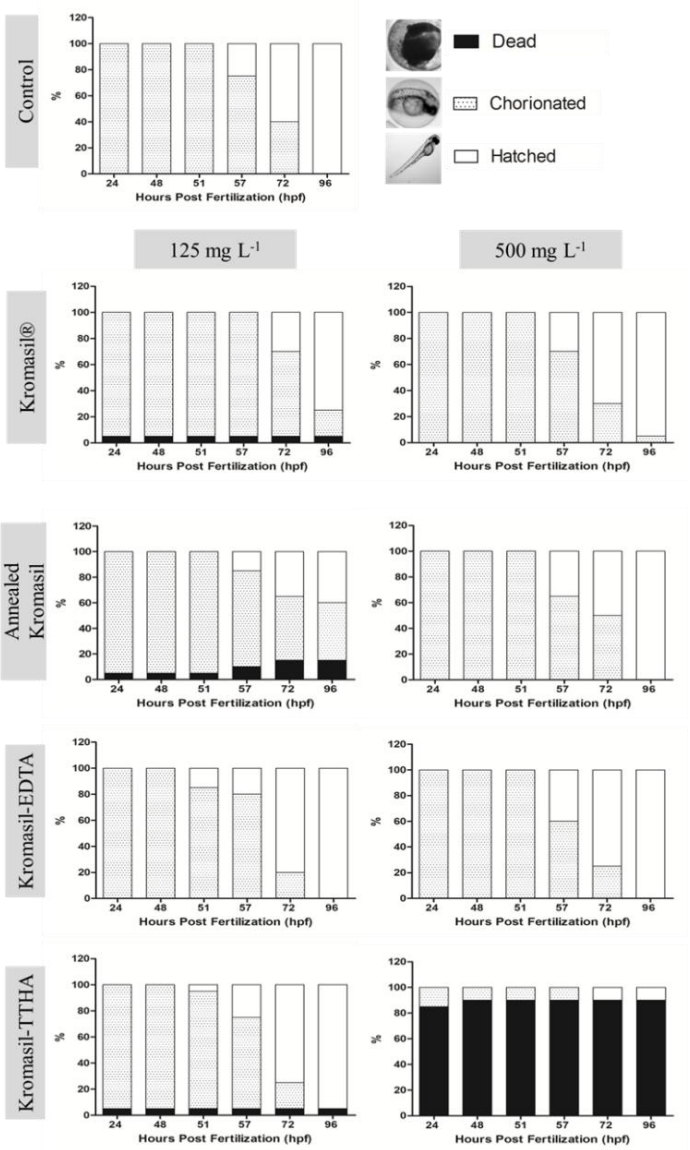

Figure 10. Zebrafish embryos development, expressed as percentages of dead, chorionated and hatched, in water containing different concentrations of MP for 24, 48, 51, 57, 72 and 96 hpf .

In case of Kromasil grafted with TTHA, exposing the embryos to 125 mg L^{-1} showed low toxicity with no changes in motility, morphology and hatching rate in compared to control. In contrast, at 500 mg L^{-1}, 85% of mortality was observed at 24 hpf embryos, which reached to 90% after 96 hpf.

4. CONCLUSIONS

APCA ligand grafted Kromasil particles could easily be produced by a facile general approach, exploiting formation of an amide bond. The grafting left the attached ligand functional in adsorption of REE cations. Produced adsorbents revealed high and element-selective capacity in the range 0.83-2.2 mmol/g and could be attractive

for applications in hydrometallurgy and recycling of REE. Cytotoxicity studies showed results that were concentration-, time-, cell- and ligand-dependent. The toxicity of ligand-grafted particles was appreciably higher, especially for Kromasil-TTHA, than that of ligand-free (annealed Kromasil) or aminopropyl functionalized particles (Kromasil®). Internalization of the MP inside the cells was observed. These data were correlated with those obtained *In vivo*. Toxicity studies in Zebrafish embryos showed no toxicity for all MP, except Kromasil-TTHA, at high concentration (500 mg L^{-1}) after 96 hpf.

ASSOCIATED CONTENT

Supporting Information. FTIR, TGA, EDS mapping results for all samples, and fitting of adsorption isotherm of Nd^{3+}-cations on Kromasil-EDTA and Kromasil-TTHA samples by Freundlich equation.

Author Contributions

The manuscript was written through contributions of all authors. All authors have given approval to the final version of the manuscript. ‡These authors contributed equally.

Funding Sources

The authors are indebted to ERA-MIN 2 MetRecycle project for support of this work financed via Swedish Research Council VINNOVA grant 2018-00739. Swedish Research Council (Vetenskapsrådet) is acknowledged for support of the project 2018-04841 Multifunctional hybrid adsorbents for water purification.

ACKNOWLEDGMENT

All authors would like to thank Nadir Bettache, Mireille Rossel and Nicolas Cubedo for their technical assistance in zebrafish experiments and the imaging facility MRI-CNRS.

REFERENCES

(1) Zhang, Y.Y. Peak Neodymium - Material Constraints for Future Wind Power Development, Master Thesis, Uppsala University, 2013; https://www.diva-portal.org/smash/get/diva2:668091/FULLTEXT01.pdf

(2) Yang, X.L.; Zhang, J.W.; Fang, H.H. Rare earth element recycling from waste nickel-metal hydride batteries, J. Hazardous. Mater., 2014, 279, 384-388.

(3) Riba, J.R.; López-Torres, C.; Romeral, L.; Garcia, A. Rare-earth-free propulsion motors for electric vehicles: A technology review, Renew. Sustain. Energy Rev., 2016, 57, 367-379.

(4) Kegl, T.; Košak, A.; Lobnik, A.; Novak, Z.; Kralj, A.K.; Ban, I. Adsorption of rare earth metals from wastewater by nanomaterials: A review, J. Hazardous Mater., 2020, 386, 121632.

(5) Izatt, S.R.; McKenzie, J.S.; Izatt, N.E.; Bruening, R.L.; Krakowiak, K.E.; Izatt, R.M. MOLECULAR RECOGNITION TECHNOLOGY: A GREEN CHEMISTRY PROCESS FOR SEPARATION OF INDIVIDUAL RARE EARTH METALS, White Paper on Separation of Rare Earth Elements, February 20, 2016, http://www.ucore.com

(6) Hu, Y.M.; Misal Castro, L.C.; Drouin, E.; Florek, J.; Kählig, H.; Larivière, D.; Kleitz, F.; Fontaine, F.G. Size-Selective Separation of Rare Earth Elements Using Functionalized Mesoporous Silica Materials, ACS Appl. Mater. Interfaces, 2019, 11, 23681–23691.

(7) Glennon, I.D.; Lynch, B.; Hall, K.; Harris, S.J.; O'Sullivan, P. Water eluent based Ion Chromatography on silica-bonded molecular baskets, in Progress in Ion Exchange: Advances and Applications, Eds. Dyer, A.; Hudson, M.J.; Williams, P.A., RSC 1995.

(8) Ohto, K.; Yano, M.; Inoue, K.; Yamamoto, T.; Goto, M.; Nakashio, F.; Shinkai, S.; Nagasaki, T. Solvent Extraction of Trivalent Rare Earth Metal Ions with Carboxylate Derivatives of Calixarenes, Analyt. Sci., 1995, 11, 893-902.

(9) Yan, B. Photofunctional Rare Earth Hybrid Materials, Springer 2017, p. 40.

(10) Hu, Y.M.; Florek, J.; Larivière, D.; Fontaine, F.G.; Kleitz, F. Recent Advances in the Separation of Rare Earth Elements Using Mesoporous Hybrid Materials, Chem. Rec., 2018, 18, 1261–1276.

(11) Nowack, B. Environmental Chemistry of Aminopolycarboxylate Chelating Agents. Environ. Sci. Technol. 2002, 36, 19, 4009-4016.

(12) Zhai, J.Y.; Bakker, E. Complexometric titrations: new reagents and concepts to overcome old limitations. Analyst. 2016, 141, 4252-4261.

(13) Ernst, E. Chelation Therapy for Peripheral Arterial Occlusive Disease. Circulation. 1997, 96, 1031–1033

(14) Clough, T.J.; Jiang, L.J.; Wong, K.L.; Long, N.J. Ligand design strategies to increase stability of gadolinium-based magnetic resonance imaging contrast agents. Nature Comm. 2019, 10, 1420.

(15) Wang, J.; Wang, Y.; Zhang, X.D.; Zhang, Z.H.; Zhang, Y. ; Kang, L.P.; Li, H. Syntheses of rare earth metal complexes with aminopolycarboxylic acids and study on structural changes: Nine-coordinated mononuclear $K_2[Dy(DTPA)(H_2O)]\cdot 6H_2O$ and binuclear $K_4[Ho_2(DTPA)_2]\cdot 4H_2O$. J. Coord. Chem. 2005, 58, 921-930.

(16) Wang, J.; Gao, G.R.; Zhang, Z.H.; Zhang, X.D.; Wang, Y.J. Syntheses and structural determinations of the nine-coordinate rare earth metal: $Na_4[Dy(DTPA)(H_2O)]2\cdot 16H_2O$, $Na[Dy(EDTA)(H_2O)_3]\cdot 3.25H_2O$ and $Na_3[Dy(NTA)_2(H_2O)]\cdot 5.5H_2O$. J. Coord. Chem. 2007, 60, 2221-2241.

(17) Adachi, G. Proposal of the partial logarithm of stability constant (PLSC) and its application to rare earth diethylenetriamine-N,N,N′,N′,N″,-pentaacetic acid (DTPA) complexes. J. Rare Earths. 2018, 36, 4, 337-448.

(18) Wang, J.; Liu, X.Z.; Wang, X.F.; Gao, G.R.; Xing, Z.Q.; Zhang, X.D.; Xu, R. Nine-coordinate rare earth metal complexes with aminopolycarboxylic acids: Mononuclear $(NH_4)_3[Tb(TTHA\text{-})]\cdot 5H_2O$ and binuclear $(NH_4)_4[Tb_2(DTPA)_2]\cdot 9H_2O$. J. Struct. Chem. 2008, 49, 75-83.

(19) Repo, E.; Warchoł, J.K.; Bhatnagar, A.; Sillanpää, M.; Heavy metals adsorption by novel EDTA-modified chitosan–silica hybrid materials. J. Colloid Interface Sci. 2011, 358, 261-267.

(20) Repo, E.; Warchoł, J.K.; Bhatnagar, A.; Mudhoo, A.; Sillanpää, M. Aminopolycarboxylic acid functionalized adsorbents for heavy metals removal from water. Water Res. 2013, 47, 4812-4832.

(21) Zhao, F.P.; Repo, E.; Sillanpää, M.; Meng, Y.; Yin, D.L.; Tang, W.Z. Green synthesis of magnetic EDTA-and/or DTPA-cross-linked chitosan adsorbents for highly efficient removal of metals. Ing. Eng. Chem. Res. 2015, 54, 1271-1281.

(22) Radi, S.; El Abiad, C.; Carvalho, A.P.; Santos, S.M.; Amparo, M.; Faustino, F.; Graça, M.; Neves, P.M.S.; Moura, N.M.M. An efficient hybrid adsorbent based on silica supported amino pentacarboxylic acid for water purification. J. Mater. Chem. A. 2018, 6, 13096–13109.

(23) Topel, S.D.; Polido Legaria, E.; Tiseanu, C.; Rocha, J.; Nedelec, J-M.; Kessler, V. G.; Seisenbaeva, G. A. Hybrid silica nanoparticles for sequestration and luminescence detection of trivalent rare earth ions (Dy^{3+} and Nd^{3+}) in solution. J. Nanoparticle Res. 2014, 16, 2783.

(24) Polido Legaria, E.; Topel, S. D.; Kessler, V. G.; Seisenbaeva, G.A. Molecular insights into the selective action of a magnetically removable complexone-grafted adsorbent. Dalton Trans. 2015, 44, 1273-1282.

(25) Dupont, D.; Brullot, W.; Bloemen, M.; Verbiest, T.; Binnemans, K. Selective Uptake of Rare Earths from Aqueous Solutions by EDTA Functionalized Magnetic and Nonmagnetic Nanoparticles. ACS Appl. Mater. Interfaces. 2014, 6, 4980−4988.

(26) Callura, J.C.; Perkins, K.M.; Noack, C.W.; Washburn, N.R.; Dzombak, D.A.; Karamalidis, A.K. Selective adsorption of rare earth elements onto functionalized silica particles. Green Chem. 2018, 20, 1515-1526.

(27) Polido Legaria, E.; Samouhos, M.; Kessler, V.G.; Seisenbaeva, G.A. Toward Molecular Recognition of REEs: Comparative Analysis of Hybrid Nanoadsorbents with the Different Complexonate Ligands EDTA, DTPA, and TTHA. Inorg. Chem. 2017, 56, 13938-13948.

(28) Polido Legaria, E.; Saldan, I.; Svedlindh, P.; Wetterskog, E.; Gunnarsson, K.; Kessler, V.G.; Seisenbaeva, G.A. Coordination of rare earth element cations on the surface of silica-derived nanoadsorbents. Dalton Trans. 2018, 47, 1312-1320.

(29) Ashour, R.M.; Samouhos, M.; Polido Legaria, E.; Svärd, M.; Högblom, J.; Forsberg, K.; Palmlöf, M.; Kessler, V.G.; Seisenbaeva, G.A.; Rasmuson, Å.C. DTPA-Functionalized Silica Nano- and Micro particles for Adsorption and Chromatographic Separation of Rare Earth Elements. ACS Sustainable Chem. Eng. 2018, 6, 6889-6900.

(30) Scientific Opinion of the Panel on Food Additives and Nutrient Sources added to Food on calcium silicate, silicon dioxide and silicic acid gel added for nutritional purposes to food supplements following a request from the European Commission. The EFSA Journal. 2009, 1132, 1-24.

(31) Asefa, Tao, T. Z. Biocompatibility of Mesoporous Silica Nanoparticles. Chem. Res. Toxicol. 2012, 25, 2265−2284

(32) Napierska, D.; Thomassen, L.C.J.; Lison, D.; Martens, J.A.; Hoet, P.H. The nanosilica hazard: another variable entity. Particle Fiber Toxicol. 2010, 7, 39.

(33) Chen, L.J.; Liu, J.; Zhang, Y.L.; Zhang, G.L.; Kang, Y.Y.; Chen, A.J.; Feng, X.L.; Shao, L.Q. The toxicity of silica nanoparticles to the immune system. Nanomedicine. 2018, 13, 1939–1962.

(34) Nan, A.; Bai, X.; Son, S.J.; Lee, S.B.; Ghandehari, H. Cellular Uptake and Cytotoxicity of Silica Nanotubes. Nano Lett. 2008, 8, 2150-2154.

(35) Vallhov, H.; Gabrielsson, S.; Strømme, M.; Scheynius, A.; Garcia-Bennett, A.E. Mesoporous Silica Particles Induce Size Dependent Effects on Human Dendritic Cells. Nano Lett. 2007, 7, 3576-3582.

(36) Fadeel, B.; Garcia-Bennett, A.E. Better safe than sorry: Understanding the toxicological properties of inorganic nanoparticles manufactured for biomedical applications. Adv. Drug Deliv. Rev. 2010, 62, 362-74.

(37) Maurer-Jones, M.A.; Gunsolus, I.L.; Murphy, C.J.; Haynes, C.L. Toxicity of Engineered Nanoparticles in the Environment. Anal. Chem. 2013, 85, 3036-3049.

(38) Duan, J.; Yu, Y.; Li, Y.; Yu, Y.; Sun, Z. Cardiovascular toxicity evaluation of silica nanoparticles in endothelial cells and zebrafish model. Biomaterials. 2013, 34(23), 5853-5862.

(39) Cheng, J.; Flahaut, E.; Cheng, S.H. Effect of carbon nanotubes on developing zebrafish (Danio rerio) embryos. Environmental Toxicology and Chemistry. 2007, 26(4), 708–716.

(40) Wehmas, L.C.; Anders, C.; Chess, J.; Punnoose, A.; Pereira, C. B.; Greenwood, J.A.; Tanguay, R.L. Comparative Metal Oxide Nanoparticle Toxicity Using Embryonic Zebrafish. Toxicol Rep. 2015, 2, 702-715.

(41) Bai, C.C.; Tang, M. Toxicological study of metal and metal oxide nanoparticles in zebrafish. J. Applied Toxicol. 2020, 40, 37-63.

(42) Strähle, U.; Scholz, S.; Geisler, R. ; Greiner, P.; Hollert, H.; Rastegar, S.; Schumacher, A.; Sel-derslaghs, I.; Weiss, C.; Witters , H.; Braunbeck, T. Zebrafish embryos as an alternative to animal experiments--a commentary on the definition of the onset of protected life stages in animal welfare regulations. Reprod Toxicol. 2012, 33, 128-32.

(43) Alothman, Z.A. A Review: Fundamental Aspects of Silicate Mesoporous Materials. Materials. 2012, 5, 2874-2902.

(44) Pogorilyi , R.P.; Pylypchuk , I.; Melnyk , I.V.; Zub , Y.L.; Seisenbaeva, G.A.; Kessler, V.G. Sol-Gel Derived Adsorbents with Enzymatic and Complexonate Functions for Complex Water Remediation. Nanomaterials. 2017, 7, 298.

(45) Kegl, T.; Ban, I.; Lobnik, A.; Košak, A. Synthesis and characterization of novel Γ-Fe_2O_3-NH_4OH@SiO_2(APTMS) nanoparticles for dysprosium adsorption, J. Hazardous Mater., 2019, 378, 120764.

(46) Ramasamy, D.L.; Khan, S.; Repo, E.; Sillanpää, M. Synthesis of mesoporous and microporous amine and non-amine functionalized silica gels for the application of rare earth elements (REE) recovery from the waste water-understanding the role of pH, temperature, calcination and mechanism in Light REE and Heavy REE separation, Chem. Eng. J., 2017, 322, 56-65.

(47) Xiao, C.L.; Zhang, A.; Chai, Z.F. Synthesis and characterization of novel macroporous silica-polymer-calixcrown hybrid supramolecular recognition materials for effective separation of cesium, J. Hazardous Mater., 2014, 267, 109-118.

(48) Zhang, A.; Wang, W.H.; Chai, Z.F.; Kumagai, M. Separation of strontium ions from a simulated highly active liquid waste using a composite of silica-crown ether in a polymer, J. Sep. Sci., 2008, 31, 3148-3155.

(49) Zhang, A.; Xiao, C.L.; Liu, Y.H.; Hu, Q.H.; Chen, C.M.; Kuraoka, E. Preparation of macroporous silica-based crown ether materials for strontium separation, J. Porous Mater., 2010, 17, 153–161.

(50) Ali, L.M.A. Toxicity studies of Polymeric based supermagnetic iron oxide nanoparticles. PhD The-sis. Universidad Zaragoza 2014. ISSN 2254-7606.

(51) Murugadoss, S.; Lison, D.; Godderis, L.; Van Den Brule, S.; Mast, J.; Brassinne, F.; Sebaihi, N.; Hoet, P.H. Toxicology of silica nanoparticles: an update. Arch Toxicol. 2017, 91(9), 2967–3010.

(52) Cocco, P.; Dosemeci, M.; Rice, C. Lung cancer among silica-exposed workers: the quest for truth between chance and necessity. Med Lav. 2007, 98, 3-17.

(53) Leung, C.C.; Yu, I.T.; Chen, W. Silicosis. Lancet. 2012, 379, 2008-2018.

(54) Park, E.J.; Park, K. Oxidative stress and pro-inflammatory responses induced by silica nanoparticles in vivo and in vitro. Toxicology Letters. 2009, 184, 18–25.

(55) Serda, R. E.; Ferrati, S.; Godin, B.; Tasciotti, E.; Liu, X.W.; Ferrari, M. Mitotic trafficking of silicon micro particles. Nanoscale. 2009, 1, 250–259.

(56) Bimbo, L. M;. Mäkilä, E.; Laaksonen, T.; Lehto, V. P.; Salonen, J.; Hirvonen, J.; Santos, H. A. Drug permeation across intestinal epithelial cells using porous silicon nanoparticles, Biomaterials, 2011, 32, 2625-2633.

(57) Pietroiusti, A.; Stockmann-Juvala, H.; Lucaroni, F.; Savolainen, K. Nanomaterial exposure, toxicity, and impact on human health. WIREs Nanomed Nanobiotechnol. 2018, 10, e1513.

(58) Pierini, D.; Bryan, N.S. Nitric oxide availability as a marker of oxidative stress. Methods Mol. Biol. 2015, 1208, 63-71.

(59) Soenen, S.J.H.; Illyes, E.; Vercauteren, D.; Braeckmans, K.; Majer, Z.; De Smedt, S.C.; De Cuyper, M. The role of nanoparticle concentration-dependent induction of cellular stress in the internalization of non-toxic cationic magnetoliposomes, Biomaterials. 2009, 30(36), 6803-6813.

(60) Handy, R.D.; Henry, T.B.; Scown, T.M.; Johnston, B.D.; Tyler, C.R. Manufactured nanoparticles: their uptake and effects on fish--a mechanistic analysis. Ecotoxicology. 2008, 17(5), 396-409.

(61) Maurer-Jones, M.A.; Gunsolus, I.L.; Murphy, C.J.; Haynes, C.L. Toxicity of Engineered Nanoparticles in the Environment. Anal. Chem. 2013, 85, 6, 3036-3049

Supplementary materials

Mesoporous silica adsorbents modified with amino polycarboxylate ligands – functional characteristics, health and environmental effects

Gulaim A. Seisenbaeva,[a] Lamiaa M.A. Ali,[b,c,d§] Ani Vardanyan,[a§] Magali Gary-Bobo[d], Tetyana Budnyak,[e,f] Vadim G. Kessler,[a] Jean-Olivier Durand[b]

a Department of Molecular Sciences, BioCenter, Swedish University of Agricultural Sciences, Box 7015, SE-75007, Uppsala, Sweden

b Institut Charles Gerhardt de Montpellier, UMR5253, Université de Montpellier, Place EugèneBataillon, CC 1700 – Bâtiment 17, 34095 Montpellier Cedex 5, France

c Department of Biochemistry, Medical Research Institute, University of Alexandria, 21561 Alexandria, Egypt.

d IBMM, Institut des Biomolécules Max Mousseron, UMR 5247 CNRS, UM-Faculté de Pharmacie, 15 Avenue Charles 9 Flahault, 34093 Montpellier Cedex 05 (France)

e Department of Materials and Environmental Chemistry, Stockholm University, Svante Arrhenius väg 16 C, 106 91 Stockholm, Sweden

f Chuiko Institute of Surface Chemistry of National Academy of Sciences of Ukraine, 17 General Naumov Str., 03164 Kyiv, Ukraine

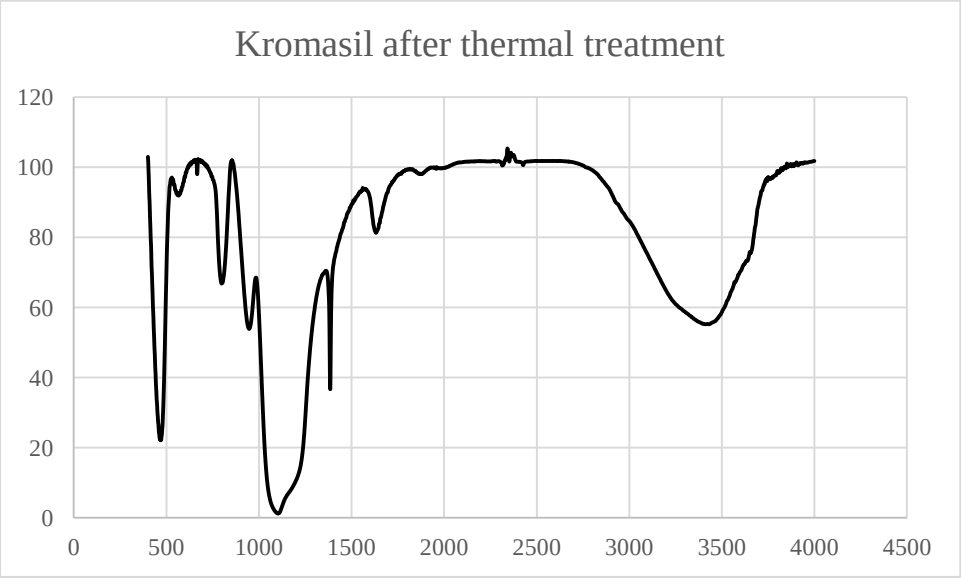

Fig. FS1 FTIR spectrum of Kromasil® thermally treated at 500°C 1h for removal of organic ligands.

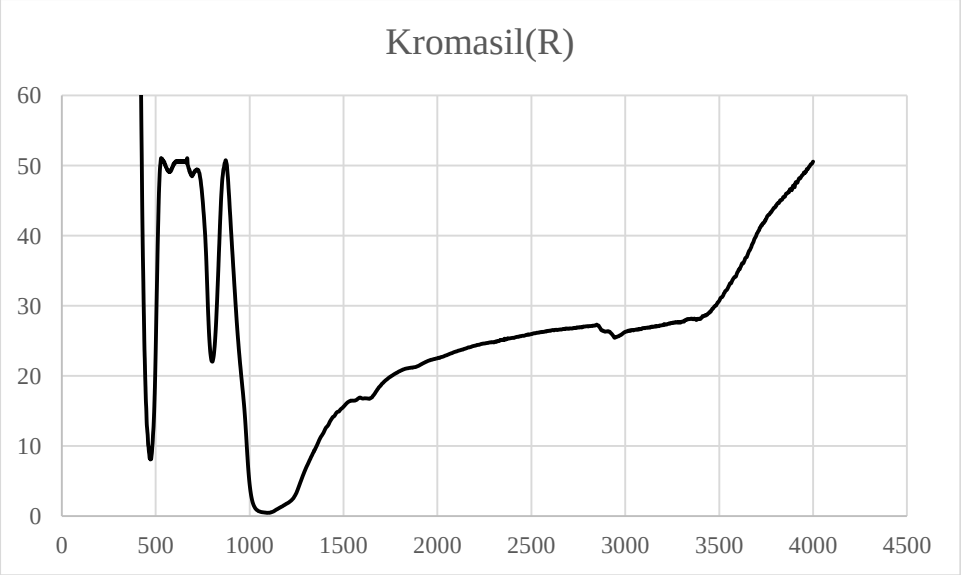

Fig. FS2 FTIR spectrum of Kromasil® bearing amino propyl ligands.

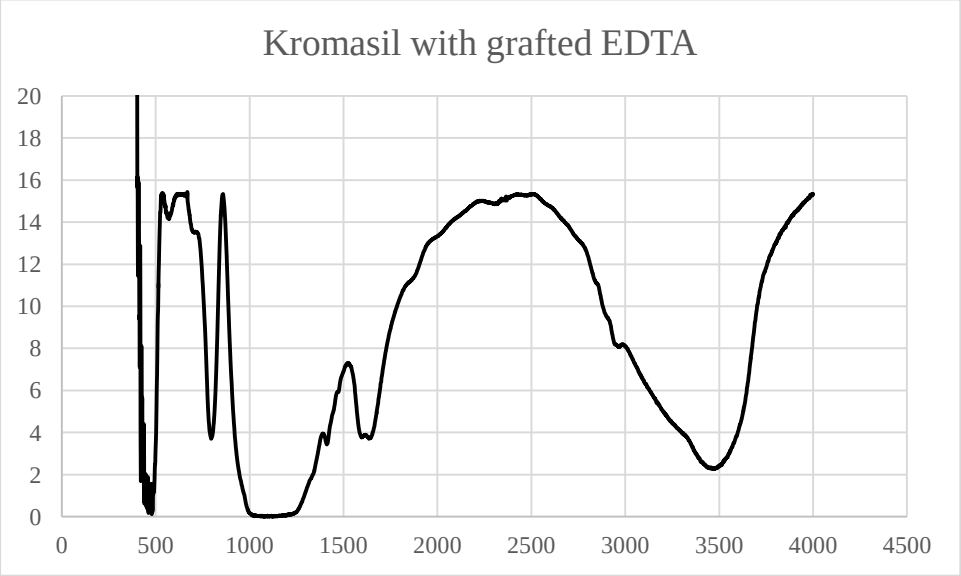

Fig. FS3 FTIR spectrum of Kromasil® modified with EDTA ligands.

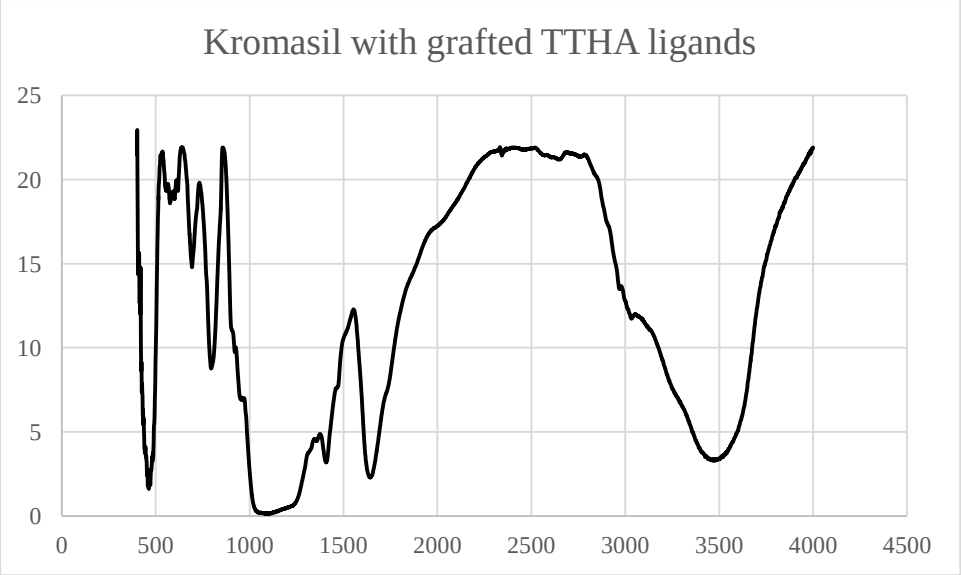

821

822 Fig. FS4 FTIR spectrum of Kromasil® modified with TTHA ligands.

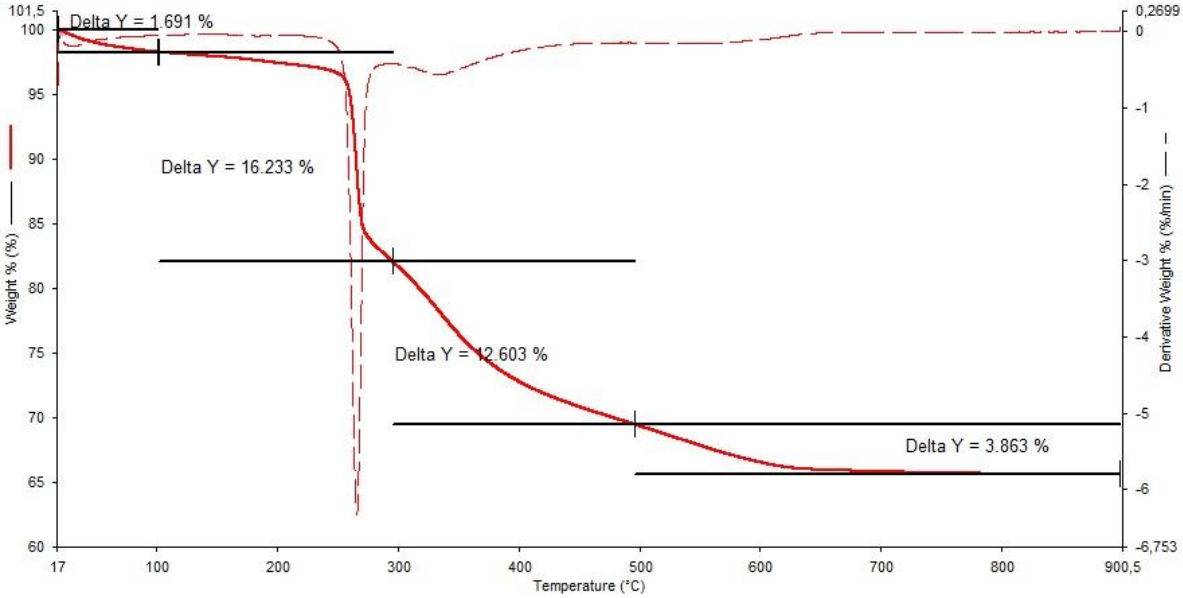

823

824 Fig. FS5 TGA of Kromasil® modified with EDTA ligands

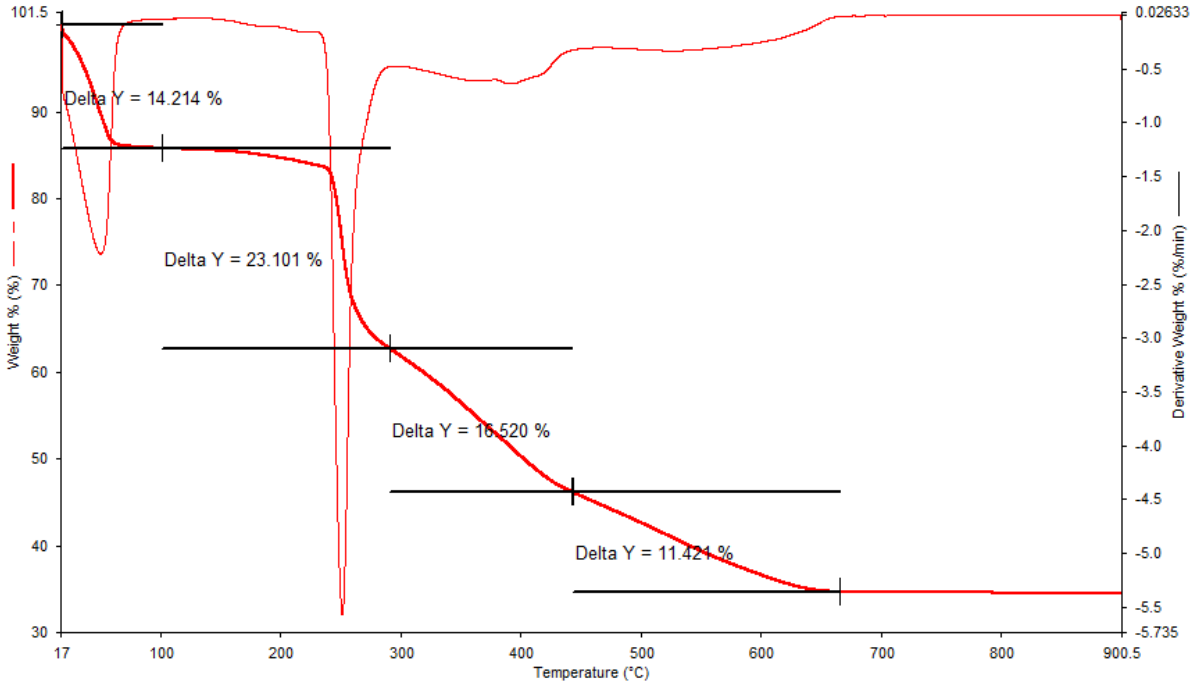

Fig. FS6. TGA of Kromasil® modified with TTHA ligands

Table TS1 Textural characteristics of materials.

Sample	S_{BET}, m^2/g	V_{pores}, cm^3/g	D_{pores}, nm
Kromasil	243	0.764	10.6
Kromasil®	188	0.654	10.0
Kromasil-EDTA	160	0.572	10.2
Kromasil-DTPA	177	0.518	8.6
Kromasil-TTHA	97	0.322	9.7

Note: S_{BET} – the Brunauer-Emmet-Teller (BET) surface area; V_{pores} – total pore volume; D_{pores} – BJH average pore diameter.

The curves of pore-size distribution by volume were obtained using the Barret-Joyner-Halenda (BJH) method [E.P. Barrett, L.G. Joyner, P.P. Halenda, The determination of pore volume and area distributions in porous substances. I. Computations from nitrogen isotherms, J. Am. Chem. Soc., 73 (1951) 373-380.] by desorption branch of the isotherms for all studied materials presented on Fig. Y. According to the IUPAC classification [W. Holleman, Lehrbuchde Anorganischen Chemie, Walter de Gruyter, Berlin, New York, 1995.] and obtained pore-size distribution (Fig. Y), all synthesized materials belong to mesoporous materials with diameter in the range from 6 – 15 nm.

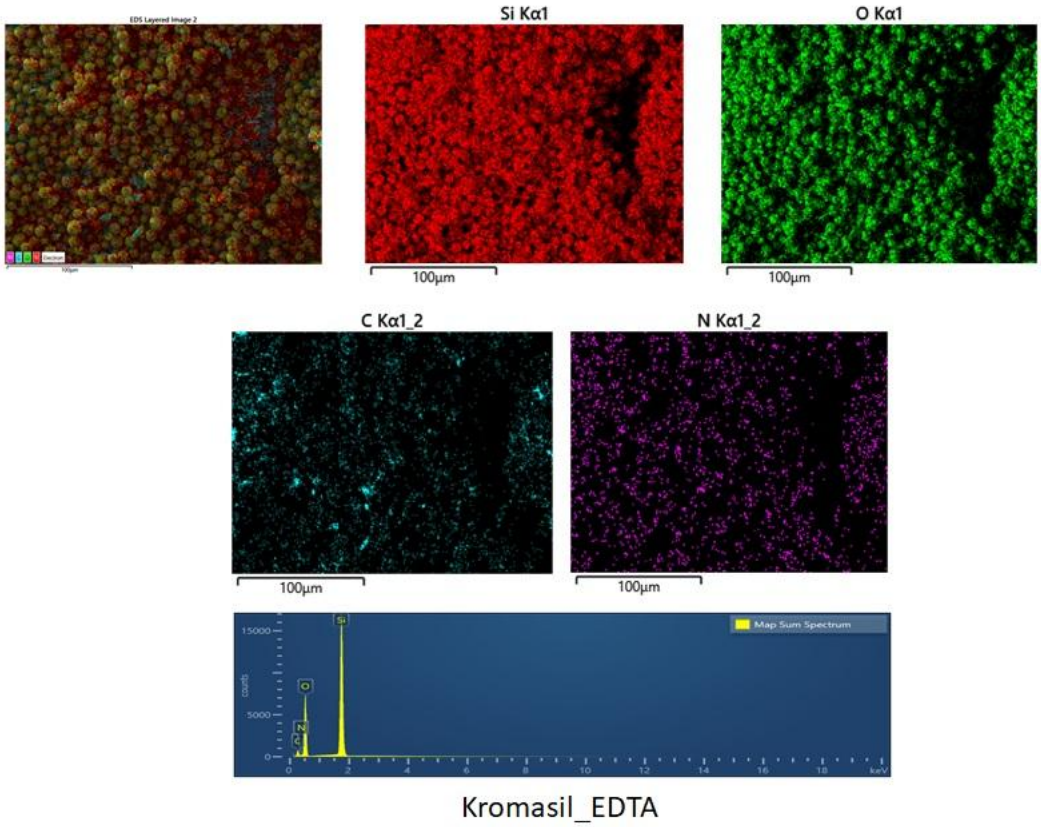

838

839 Fig. FS7. Element mapping and average X-ray emission spectrum for the Kromasil®
840 modified with EDTA ligands

841 Table TS2 EDAX analysis of the Kromasil® modified with EDTA ligands

Map Sum Spectrum				
Element	**Line Type**	**Weight %**	**Weight % Sigma**	**Atomic %**
O	K series	48.87	0.39	53.48
Si	K series	32.63	0.27	20.34
C	K series	14.70	0.45	21.44
N	K series	3.80	0.47	4.75
Total		100.00		100.00

842

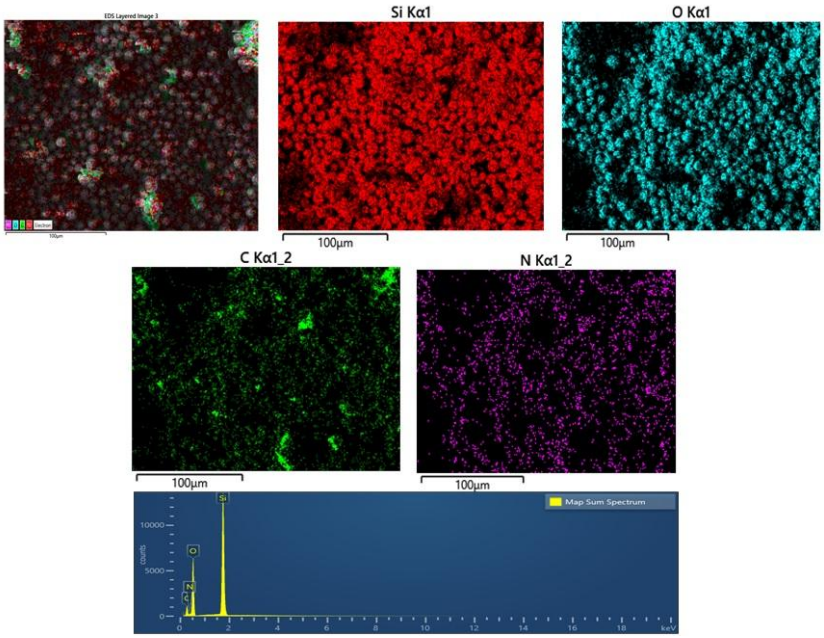

Fig. FS8. Element mapping and average X-ray emission spectrum for the Kromasil® modified with TTHA ligands

Table TS3 EDAX analysis of the Kromasil® modified with TTHA ligands

Map Sum Spectrum				
Element	**Line Type**	**Weight %**	**Weight % Sigma**	**Atomic %**
O	K series	47.32	0.43	49.53
Si	K series	27.49	0.26	16.39
C	K series	19.98	0.46	27.85
N	K series	5.21	0.55	6.22
Total		100.00		100.00

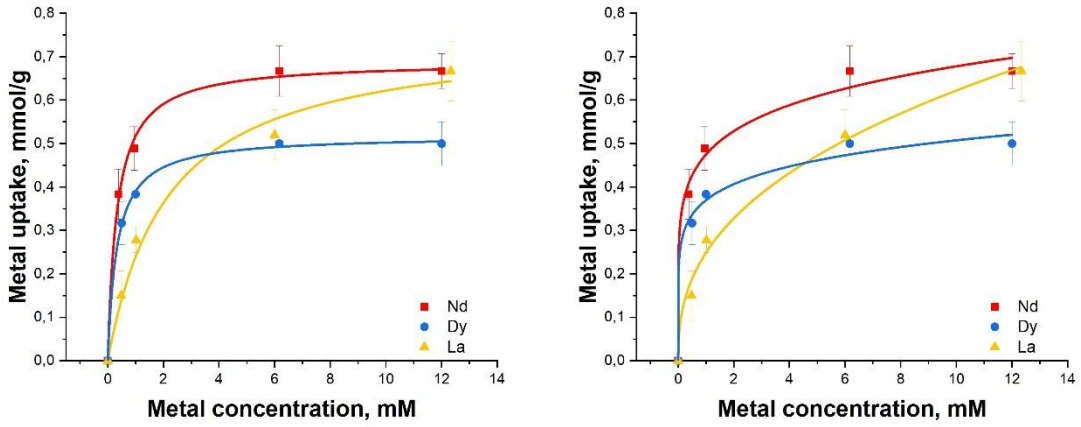

Fig. FS9 REE adsorption isotherms by Kromasil® MP. Langmuir isotherms – upper image, Freundlich isotherms – lower one.

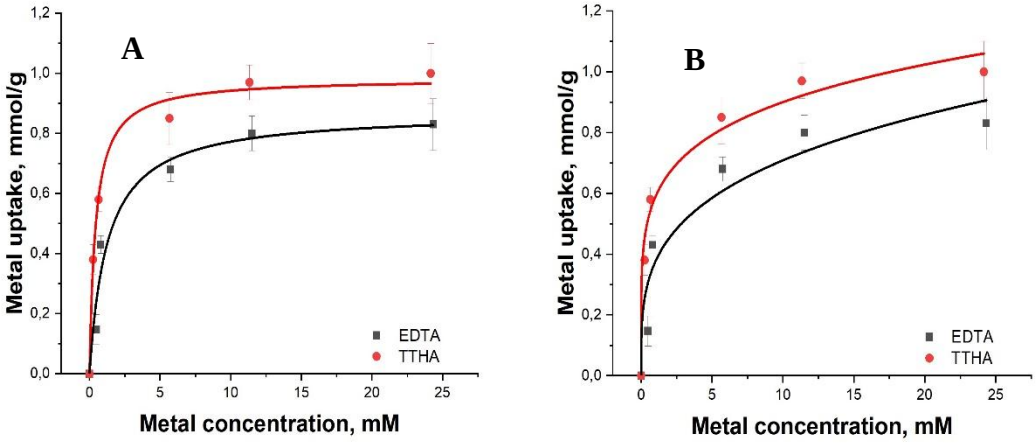

Fig. FS10 Adsorption isotherms of Nd^{3+} on Kromasil-derived adsorbents modified with amino polycarboxylate ligands: A-Langmuir isotherms, B-Freundlich isotherms.

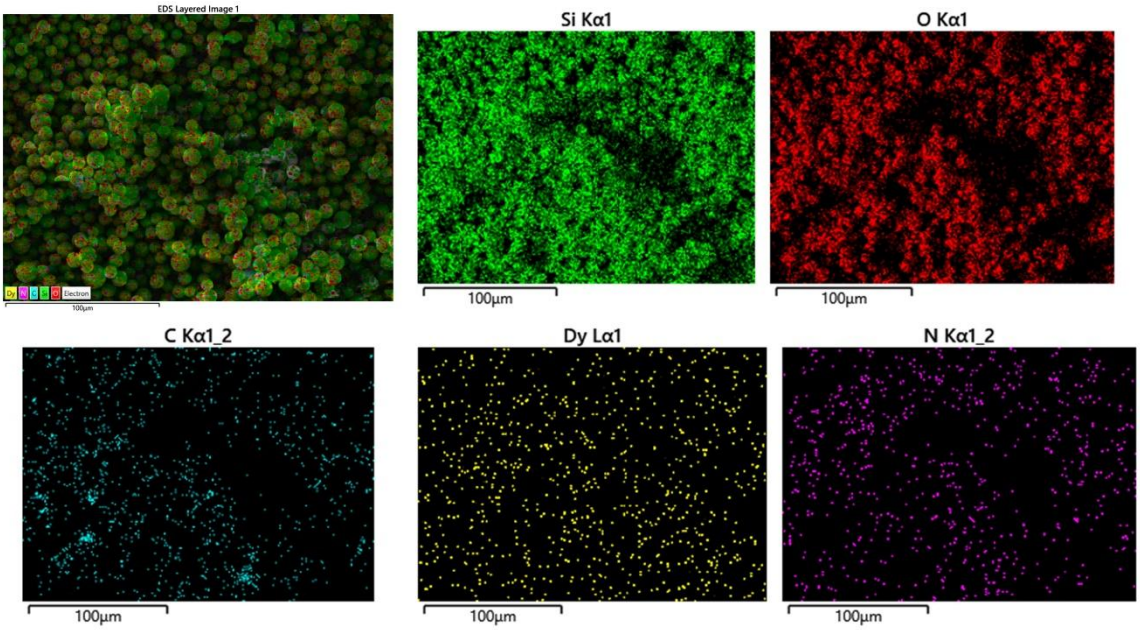

Fig. FS11 EDS mapping of Kromasil® modified with EDTA ligands after uptake of Dy^{3+} cations.

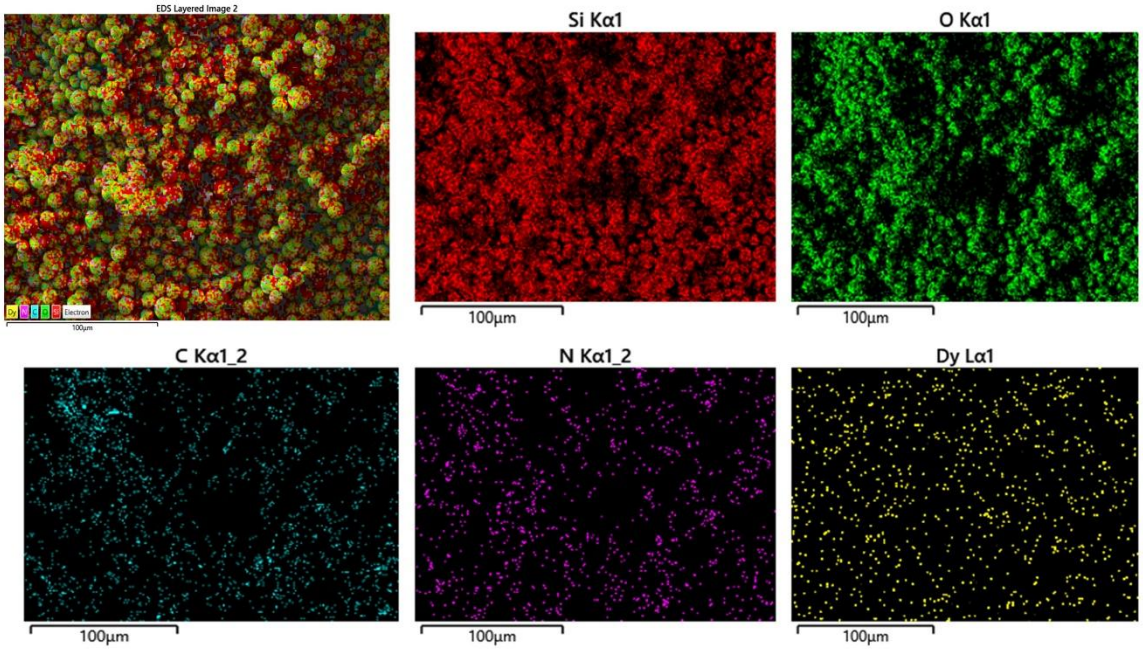

Fig. FS12 EDS mapping of Kromasil® modified with TTHA ligands after uptake of Dy^{3+} cations.

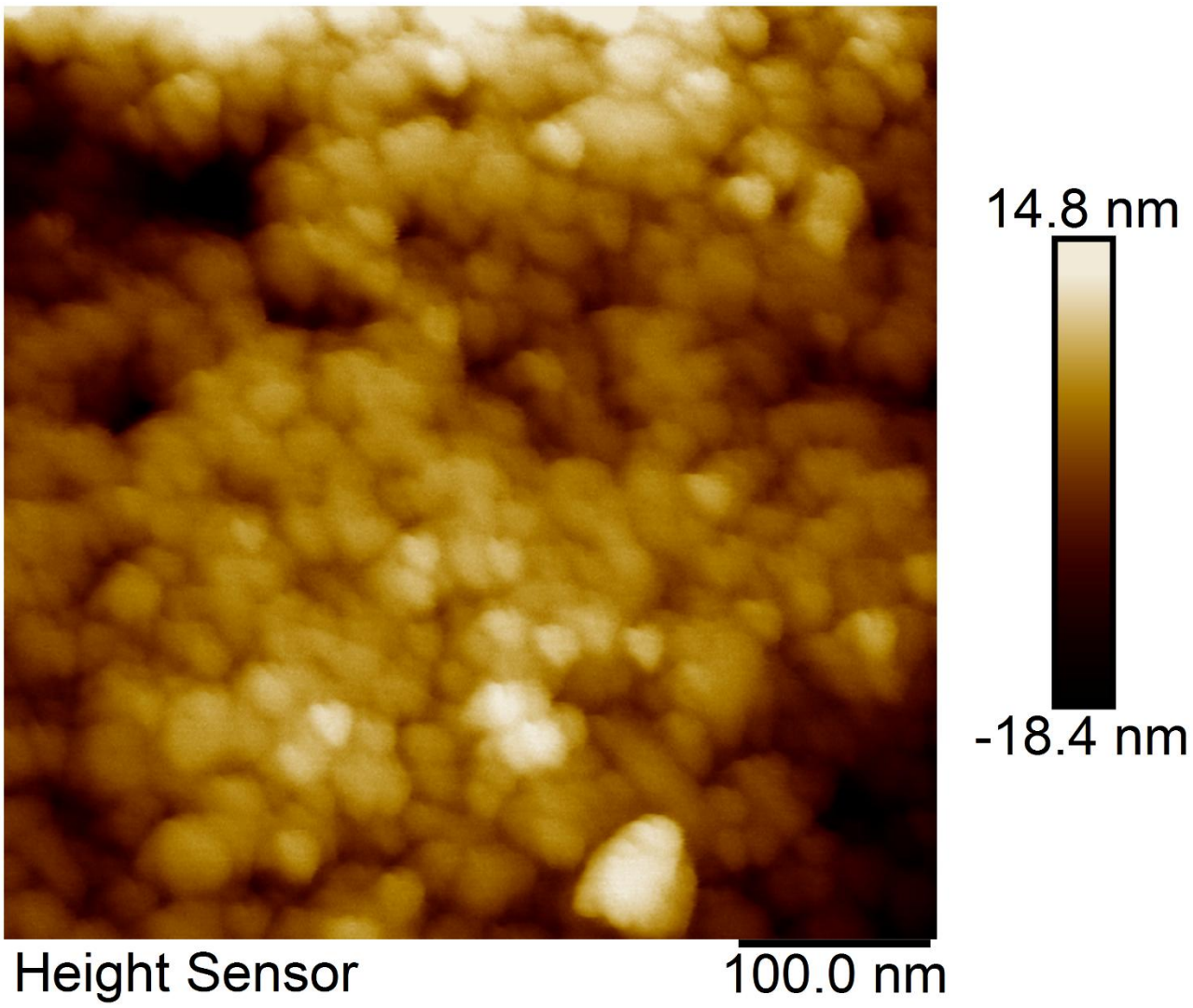

Fig. FS13 Representative high resolution AFM image of Kromasil showing the partly fused 20-30 nm nanoparticles building up the Kromasil MP.

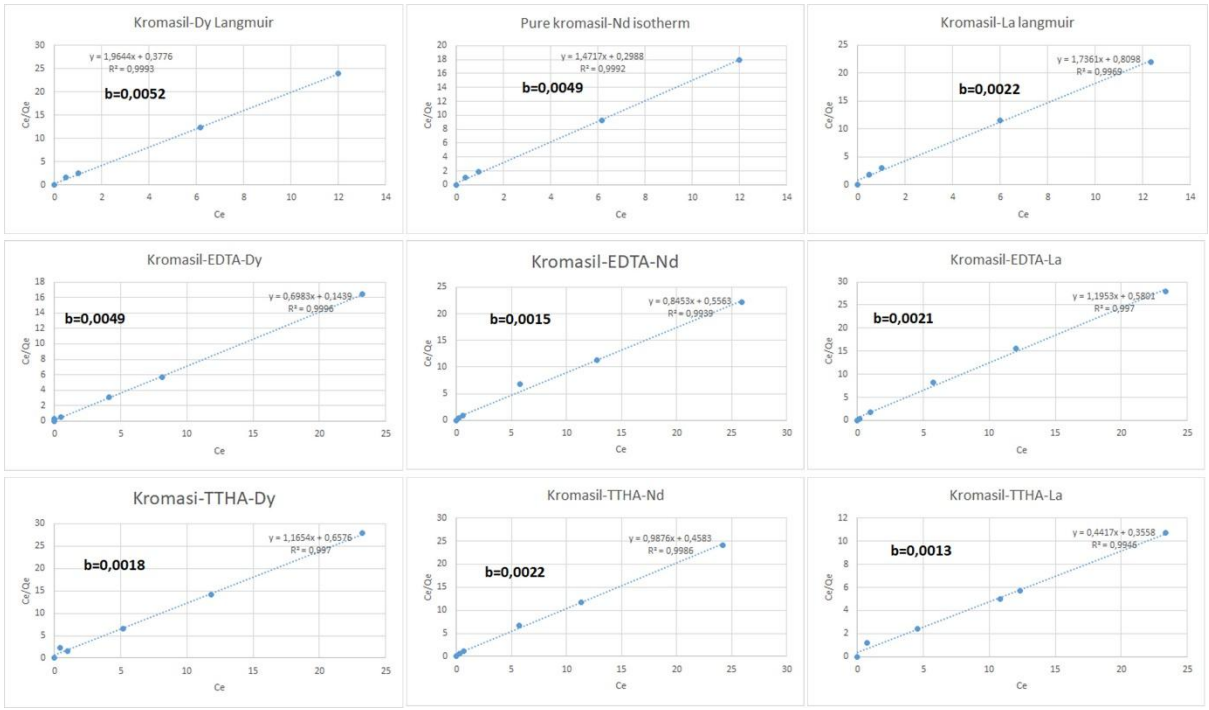

867

868 Figure FS14. Linearized plots of Langmuir adsorption isotherms (b-value is given in
869 L/mg units).